Please cite the Published Version

Contact size effects on the friction and wear of amorphous carbon films

Ben D. Beake [a],[*], Sam J. McMaster [b], Tomasz W. Liskiewicz [c],[*]

[a] *Micro Materials Ltd, Willow House, Yale Business Village, Ellice Way, Wrexham, LL13 7YL, UK*
[b] *Functional Materials and Chemistry Research Group, Coventry University, Priory Street, Coventry, CV1 5FB, UK*
[c] *John Dalton Building, Faculty of Science and Engineering, Manchester Metropolitan University, Chester Street, Manchester, M15 6BH, UK*

ARTICLE INFO

ABSTRACT

Since different properties of coating systems influence their friction and wear at different length scales contact size can play a critical role in microtribological experiments. In this study the behaviour of 3 different types of coating system which vary in terms of their thickness, substrate and mechanical properties has been investigated. The coatings were chosen for either their industrial relevance in automotive or MEMS applications, or as model coating systems. A wide range of nano/microtribological tests have been performed with different indenter geometries (tip sharpness), including single and repetitive scratch tests with unidirectional contact, and reciprocating wear tests, with depth and friction evolution monitored so that the relationships between failure mechanism and friction in coating systems with differing mechanical properties could be explored. The influence of surface topography on friction has been shown in ramped and constant load scratch tests. When fracture occurred resulting in a sudden increase in probe depth there was an abrupt decrease in friction which is ascribed to a contact area effect. In contrast, where deformation progressed through micro-wear a more gradual increase in depth can be associated with higher contact area and higher friction.

1. Introduction

Diamond-like carbon (DLC) refers to a family of metas amorphous carbon coatings whose properties vary depending on their sp^2/sp^3 ratio [1,2], level of hydrogenation and presence of doping elements. The sp^3 ratio is directly related to the ion bombardment energy during deposition [3]. Generally, amorphous carbon coatings can have up to 60% hydrogen within their structure [4]. Erdemir [5] found that the presence of absence of hydrogen drastically changes the tribological performance of DLC films.

A general naming convention exists for amorphous carbons with amorphous carbon (a-C), it's hydrogenated variant (a-C:H), the highest sp^3 content containing ta-C and its respective hydrogenated variant (ta-C:H) [6–9]. The key parameters for these films are the sp^3 content, the sp^2 clustering, orientation of the sp^2 phase, cross-sectional structures and H content [6]. The clustering of the sp^2 phase can altering the optical, electronic and mechanical properties of films with the same sp^3 and H content [4].

The properties of carbon films can be further modified by the doping of various elements into its structure during deposition. Doing so can alter properties such as thermal stability, adhesion and internal stress [10]. Tungsten has been explored a dopant for DLCs displaying excellent adhesion and tribological properties despite its reduced hardness (increased sp^2 fraction) in comparison to other DLCs [11–13]. In graphitic-like carbon (GLC), tungsten doping improves the hardness, adhesion, elasticity and toughness of the film [14]. Silicon is another popular dopant with relatively good wear resistance, adhesion and increased temperature resistance [10,15–19]

The structural parameters discussed above can hugely affect the mechanical properties of an amorphous carbon films [8,20,21]. Hainsworth and Uhure [8] compared the properties of different DLCs noting that hard a:C—H variants can have a range of hardness values from 10 to 20 GPa. Ohtake et al. [22] performed a similar comparison and noted that a-C:H can vary from 9 to 25 GPa. The relation between hardness (*H*) and elastic modulus (*E*) is well known to be a predictor of both friction and wear performance [23–27]. *H/E* and H^3/E^2 are the two main metric used in this regard [23–25]. H/E represents the elastic strain to break or (strain to failure) [23,24] whereas H^3/E^2 relates to contact yield pressure as derived from Hertzian contact analysis [23,28] with larger values indicating a higher resistance to plasticity.

These amorphous carbon films are favoured for their high hardness, wear resistance, low friction coefficient, chemical stability and high

---

biocompatibility [9]. Due to these properties, DLCs see wide use in engineering and medical fields [29–31] examples of which are as coatings on razor blades, cutting tools and protective coatings for internal combustion engines [8,32–34]. Ultra-thin (sub 100 nm) DLCs have proven useful for protecting silicon MEMS devices [35,36].

Adhesion of DLC films is a key property to increase their usability in the future; their high residual stresses can limit their applicability in extreme environments [12,37–40]. Interlayer designs and multi-layer structures have been used to increase DLC adhesion [13,38,40–42]. Additionally, bias voltage control during deposition has been used to control the stress of films to limit delamination [43,44]. Figueroa and co-workers [44–48] have produced numerous studies exploring silicon containing adhesion layers to improve DLC adhesion on steel.

The tribological performance of DLC films is heavily dependant upon the structure of the film itself and the environment in which they are operating. Humidity plays a key part in this change in performance due to the interaction with an dangling hydrogen bonds on the surface [29,49]. DLCs are also noted to form a carbonaceous transfer layer, which is graphitic in nature and can further reduce the coefficient of friction during sliding [21,49–52]. DLCs have also been noted to be able to achieve superlubricity in tribological interactions with 2D materials [53–55].

To properly assess nanoscale friction and wear, a single asperity approach is often taken thereby increasing the contact pressures but more accurately modelling the real area of contact [56]. Under these simplified contact conditions, topography can play a significant role in controlling the friction response. Santner and co-authors [57–60] have analysed the effect of topography of friction response and how subsequent surface modification can influence the friction signal. A number of authors have studied how topography affects both the growth dynamics of DLC films and their wear highlighting the importance of deposition characteristics on the surface roughness of deposited films and deleterious effect of high surface roughness on wear [9,61–66].

Nano-scale wear has been explored in the form of nano-fretting and nano-scratch tests demonstrating mechanisms that features a high degree of surface topographic change [67–70]. The effect of length scale has been explored by Achanta and co-authors [71–73]; they found that on the nano-scale (where the pressure distribution applied by atomic force microscopy is smaller than the meso- and macro-scale and single asperity interactions dominate), surface roughness effects dominate the friction trace. Furthermore, the measured coefficient was smaller as nano-scale friction has increased effects of adhesion and molecular interactions rather than deformation and third body influences [71–74]. Atomic force microscopy (AFM) is often seen employed in the measurement of surface roughness and topography [66,75–78] in addition to its use as a tribometer [73,79].

On this length scale, where low friction coefficients are typical, any angular misalignment may need to be carefully corrected as the misalignment will cause drift in the friction signal [80].

To compliment fundamental nano-scale experimental tribological investigations, molecular dynamics simulations are employed. Moseler et al. [81] have investigated the ultra smoothness of DLC surfaces through growth dynamics. Similar studies have also been performed by Neyts et al. [82], Ma et al. [83] and Li et al. [84]. Other areas of study using this technique are simulations of the tribochemical interactions of hydrogen bonds [85] and stress reduction mechanisms of doping [86].

Friction can be deconvoluted into ploughing and interfacial components as shown in Eq. (1) [87–89].

$$\mu_{total} = \mu_{ploughing} + \mu_{interfacial} \tag{1}$$

Since different properties influence friction and wear at different length scales contact size can play a critical role in microtribological experiments.

In this study we have investigated the behaviour of 3 different types of coating system which vary in terms of their thickness, substrate and

mechanical properties. The coatings were chosen for either their industrial relevance in automotive or MEMS applications, or as model coating systems.

A wide range of nano/microtribological tests have been performed with different indenter geometries (tip sharpness), including single and repetitive scratch tests with unidirectional contact, and reciprocating wear tests, with depth and friction evolution monitored so that the relationships between failure mechanism and friction in coating systems with differing mechanical properties could be explored.

2. Experimental

2.1. Coating systems

80 nm ta-C film was deposited on Si(100) under floating bias using an industrial filtered cathodic vacuum arc system (Nanofilm Technologies Pte. Ltd., Singapore) evacuated to a base pressure lower than 1×10^{-6} torr. The cathode was a 70 mm diameter, 99.999% pure graphite target mounted onto a water-cooled copper block. The arc current was ~70 A. The silicon substrates were ultrasonically cleaned with deionized water for 10 min, followed by drying with a static neutralizing blow off gun. Prior to deposition, the silicon surface was sputtered by an argon ion beam from a dc ion beam source for 3 min to remove the native oxide [35,90]. 450 nm and 962 nm DLC films were deposited on Si without an adhesion-promoting interlayer by electron cyclotron resonance (ECR) plasma chemical vapour deposition (CVD) at BAM, Germany [91]. They provided a suitable model system for studying parameter sensitivity since they delaminated consistently exhibiting small test-to-test variation in critical loads.

Multilayer coatings with un-doped DLC or Si-doped DLC top layers were deposited on hardened M2 tool steel with a plasma enhanced CVD (PECVD) Flexicoat 850 system (Hauzer Techno Coating, the Netherlands) [13,92,93]. A WC/C commercial coating, Balinit C Star, was deposited on hardened M2 tool steel by Oerliken Balzers. According to the manufacturer specification, this is applied in a single-pass vacuum process resulting in a homogeneous coating with multilamellar structure with WC-rich/C-rich phases alternating every few atomic layers [94]. There is a hard CrN sub-layer for load support and improved adhesion to the steel substrate. In the DLC and Si-DLC coating systems the adhesion layer is a 300 nm Cr and then gradient tungsten carbide layers are applied to adapt the elastic modulus of the soft substrate to the elastic modulus of the hard top coating, improving of the coating's ability to resist both abrasive and impact fatigue wear. The Cr layer was deposited using magnetron sputtering, while the WC layer was deposited using magnetron sputtering with the gradual introduction of Acetylene gas to the complete PECVD stage, thus creating a functional gradient layer in one continuous deposition process. The Si-DLC was doped with silicon using hexamethyldisiloxane (HDMSO) precursor. Layer thicknesses were:- DLC = 0.3 μm Cr/0.7 μm, W-C:H/2.9 μm, a-C:H; Si-DLC = 0.3 μm, Cr/0.7 μm, W-C:H/2.8 μm, Si-a-C:H; WC/C = 1 μm CrN/2 μm a-C:H:W.

2.2. Nanomechanical and microtribological testing

Nanomechanical properties and microtribological behaviour of the studied coatings were determined with NanoTest systems (Micro Materials Ltd., Wrexham, UK) under normal laboratory conditions (T ~22 °C; RH ~50%). Instrument and indenter calibration was performed in accordance with ISO14577 [95]. Diamond Berkovich indenters were used to perform the nanomechanical property measurements. Coating-only hardness and elastic modulus (i.e. values independent of substrate) were determined in the NanoTest software from nanoindentation data according to the approach of ISO 14,577–4 [96]. For the elastic modulus determination indentations were performed to a range of indentation depths and extrapolating the results to zero penetration depth to obtain a result free of substrate influence. For hardness the value at $h_c/t_c = 0.1$ (h_c = contact depth, t_c = film thickness) was

taken to achieve a fully developed plastic zone in the coating without substrate plasticity.

Nano- and micro-scale scratch tests were performed as 3-pass procedures involving a pre-scan surface profile, ramped load scratch and post-scan surface profile that were subsequently analysed in the NanoTest software to determine the on-load and residual depth data, following the approach described in CEN/TS 17,629 [97]. Spheroconical diamond probes with a range of end radii were employed, as summarised in Table 1 [35,36,90]. The end radii were calibrated by nanoindentation testing over a wide load range on fused silica and sapphire (0001) reference samples.

Simulated stress distributions of the von Mises, normal and interfacial stresses developed at different applied loads in scratch tests on DLC, Si-DLC and WC/C coatings on hardened M2 steel were generated using the Surface Stress analyzer (SIO, Rugen, Germany) [98]. The input parameters were (i) mechanical properties of the coating (taken as monolayered) and substrate, i.e. *H, E* and *H/Y* (*H/Y* = 1.2 for coatings, *H/Y*

= 2.5 for the steel substrate) (ii) coating thickness (iii) Poisson's ratios (iv) probe radius, applied load and measured friction coefficient in the nano-scratch test.

Multi-pass (repetitive) nano-scratch tests were performed including pre- and post- topographical scans in addition to the constant load scratch tests, and analysed by the same methodology as the ramped load scratch tests. The general approach has been summarised previously in [33,89]. Regarding the critical load points described below: (i) L_y = critical load for onset of non-elastic deformation (yield load); (ii) L_{c1} = critical load for cracking; (iii) L_{c2} = critical load for total film failure [33]. This was used for all the coating systems tested in this work.

Nano-fretting tests were performed with a NanoTest Vantage system (Micro Materials Ltd., Wrexham, UK) using 5 and 37 μm diamond probes. The configuration for nano-fretting includes an additional oscillating stage with a multi-layer piezo-stack to generate sample motion. The piezo movement is magnified by means of a lever arrangement to achieve larger amplitudes [99]. The fretting track length was set at 10 μm for the ta-C film and 7 μm for the DLC, Si-DLC and WC/C coatings. The oscillation frequency was 5 Hz. Tangential (friction) force data were acquired simultaneously with depth data throughout the nano-scratch and fretting tests using a lateral force transducer which was calibrated by a method of hanging masses. Friction coefficients during the fretting tests were determined from friction loops by the method of Burris and Sawyer to eliminate any potential transducer misalignment issues [80].

A NanoTest Vantage fitted with a NanoTriboTest module including a reciprocating stage (PI, Germany) controlled within the NanoTest software was used for the reciprocating tests on the DLC, Si-DLC and WC/C coatings. 500-cycle reciprocating wear tests were performed at 10–500 mN with a diamond indenter of 25 μm end radius as the test probe, 1 mm track length and maximum sliding velocity of 0.5 mm/s. The sliding velocity was at its maximum over the central 90% of the track and linearly reduced to zero at the turn-around points. The total sliding distance was 1 m. The friction coefficient in the reciprocating tests was determined from the frictional energy dissipation as shown by Fouvry and Liskiewicz [100–102].

$$\mu = \frac{Frictional\ energy\ dissipation}{2 \times actual\ track\ length \times applied\ load} \tag{2}$$

The tests performed on each coating, applied load, number of cycles under load and the probe radii are summarised in Table 1.

3. Results

3.1. Mechanical properties

The mechanical properties of the coatings are summarised in Table 2. The approach described in ISO14577–4 was adopted to obtain values that were independent of the hardness or modulus of the substrates (Si (100) *H* = 12.5 GPa, *E* = 165 GPa; hardened M2 tool steel *H* = 12 GPa, *E* = 210 GPa). The thinner soft DLC coating system appeared significantly more resistant to indentation due to the enhanced load support from the harder and stiffer silicon substrate but the ISO approach shows that it is only slightly harder and stiffer than the thicker coating.

Table 1
Summary of nano/micro-tribological tests.

(a) 450 and 962 nm soft DLC on Si					
Coating	Test	*R* (μm)	Load (mN)	Cycles under load	Scratch length (μm) **
450 nm	Nano-scratch	3.7	Ramped to 100	1	150
450 nm	Repetitive nano-scratch	3.7	40,50,60	10	300
450 nm	Nano-scratch	6.5	Ramped to 300*	1	1000
450 nm	Repetitive nano-scratch	6.5	84–170	20	1000
962 nm	Nano-scratch	3.7	Ramped to 100	1	150
962 nm	Nano-scratch	6.5	Ramped to 150*	1	400
962 nm	Repetitive nano-scratch	6.5	60,70,80	20	1000

(b) 80 nm ta-C on Si				
Test	*R* (μm)	Load (mN)	Cycles under load	Track length (μm)
Nano-scratch [90]	1.1	Ramped to 18	1	100
Nano-scratch [36]	3.1	Ramped to 160	1	150
Nano-scratch [35]	4.6	Ramped to 200*, 300	1	300*
Nano-scratch [36]	9.0	Ramped to 500	1	150
Nano-fretting [35]	5	10	1500–18,000	10
Nano-fretting [35]	37	200	300–18,000	10

(c) DLC, Si-DLC, WC/C coatings on hardened M2 steel				
Test	*R* (μm)	Load (mN)	Cycles under load	Track length (μm)
Nano-scratch [13]	5	Ramped to 500	1	500
Micro-scratch [13]	25	Ramped to 5000	1	1000
Nano-fretting [137]	5	100	4500	7
Reciprocating wear [125]	25	10–500	500	1000

*Tests were carried out at x100 different loading rates and scan speeds but at the same *dL/dx*.

** For both ramped and constant load scratches, this length includes a 50 μm distance utilised for levelling in the data processing procedure.

* Tests to 200 mN were performed over a range of *dL/dx*, track lengths varied in the range 150–850 μm. The track length was determined by the scan speed and loading rate.

Table 2
Coating mechanical properties* and surface roughness**.

	H (GPa)	*E* (Gpa)	*H/E*	H^3/E^2 (Gpa)	R_a (nm)
80 nm ta-C	23.9	331	0.072	0.125	3.1
450 nm soft DLC	4.4	31.6	0.139	0.085	1.9
962 nm soft DLC	4.1	28.5	0.144	0.085	1.9
3.8 μm DLC	23.4	234	0.100	0.234	10.3
3.9 μm Si-DLC	16.8	151	0.111	0.208	10.9
3.0 μm W-DLC	13	149	0.087	0.099	11.3

* Coating only (substrate free) values determined by applying ISO14577–4.
** Surface roughness was measured from the initial topography scan in the 3-pass scratch tests (topography-scratch-topography).

3.2. Ramped and repetitive nano-scratch tests on 450 and 962 nm DLC films

Tables 3a,b) show that the critical loads for cracking and total film failure were much higher for the thinner coating. Table 3a shows the influence of a 100-fold change in loading rate with concurrent change in scan speed, i.e. the tests were done at the same dL/dx, on the critical loads. The Table shows that this change resulted in only a 10% increase in the L_{c1} and L_{c2} critical loads. The influence of probe sharpness on the critical loads in the nano-scratch tests are shown in Table 3b. The variation in scratch recovery at failure is shown in Table 3c. The scratch recovery (SR) is defined in an analogous way to elastic recovery in a nanoindentation test (Eq. (3)).

$$Scratch\ recovery = \frac{100\% \times (maximum\ depth - residual\ depth)}{maximum\ depth} \quad (3)$$

Repetitive constant load scratch tests were performed at sub-critical loads (i.e. below L_{c1}). An illustrative example at 70 mN on the 962 nm coating is shown below (Fig. 1). In this example there were 41 cycles, of which 20 were under load ("S") and 21 were topographic ("T"). For the on-load cycles the load was linearly ramped after 50 μm scan distance reaching 70 mN just after 250 μm, remaining at this level until the end of the track and then the probe was removed and placed at the start of the track for the next pass (a topography scan) following a procedure described in [89,97,103]. The cycles were T-S-T-S….T. In Fig. 1 (a,b) only selected cycles are shown for clarity. Data are shown after correction for slope, instrument frame compliance and surface topography. In this example the film fails over only part of the track in one cycle (cycle 11) with progressively more of the film failing with each subsequent cycle. There is appreciable debris generation once the coating fails, which precludes the probe reaching the bottom of the track along its length until this debris is ploughed out with continued on-load scratch cycles.

The mean depth values averaged over entire constant load region provide a convenient graphical method to monitor the evolution of the film failure [89,97]. The evolution in the on-load depth (h_t) and residual depth (h_r) with continued scratch cycles from typical tests at 60–80 mN is shown in Fig. 2(a). Since L_{c1} ~98 mN in ramped scratch tests with the same loading rate and scan speed (Table 3(a)) these tests were performed at fractional loads (L/L_c) of 0.61–0.82. At 60 mN contact was almost elastic after 20 scratches but film failure occurred within 20 cycles for the tests at higher load. Fig. 2(b) shows SR vs. cycles. SR gradually decreased over the first few cycles as the on-load depth was almost constant but the residual depth gradually increased. Friction coefficient vs. cycles is shown in Fig. 2(c).

Fig. 3(a-b) show the load dependence of the number of cycles to the onset of film failure, defined as the beginning of cracking in part of the track revealed in the on-load depth and friction data. For tests close to the L_{c1} (at fractional loads near to 1) abrupt film failure typically occurred within a single cycle over the entire region of the scratch track under constant load (i.e. from 260 to 1000 μm).

Table 3a
Influence of loading rate and scan speed on the critical loads for soft DLC films on Si.

Coating	Loading rate (mN/s)	Scan speed (μm/s)	L_{c1} (mN)	L_{c2} (mN)
450 nm	0.167	0.5	170 ± 14	172 ± 14
962 nm	0.167	0.5	94 ± 1	102 ± 1
450 nm	1.67	5	182 ± 5	184 ± 5
962 nm	1.67	5	98 ± 1	107 ± 1
450 nm	16.7	50	192 ± 4	193 ± 3
962 nm	16.7	50	105 ± 0	113 ± 2

[R = 6.5 μm; data previously reported in Nanoindent+ [91, 98]].

Table 3b
Variation in critical load and friction with probe radius on soft DLC coatings.

Coating	R (μm)	L_y (mN)	μ at L_y	L_{c1} (mN)	μ at L_{c1}	L_{c2} (mN)	μ at L_{c2}
450 nm	3.7	6 ± 1	0.03	69 ± 1	0.09	72 ± 2	0.09
450 nm	6.5	20 ± 2	0.08	182 ± 5	0.11	184 ± 5	0.11
962 nm	3.7	8 ± 4	0.03	50 ± 5	0.07	57 ± 4	0.10
962 nm	6.5	27 ± 3	0.08	98 ± 1	0.10	107 ± 1	0.11

Table 3c
Variation in scratch recovery with probe radius on soft DLC coatings.

Coating	R (μm)	% Scratch recovery at L_{c1}	% Scratch recovery at L_{c2}
450 nm	3.7	67	65
450 nm	6.5	70	70
962 nm	3.7	79	69
962 nm	6.5	92	80

3.3. Nano-scratch and nano-fretting tests on ta-C

The influence of probe radius on the critical loads and friction coefficient at these in nano-scratch tests on 80 nm ta-C is summarised in Table 4. Clear film failure and substrate exposure occurred at L_{c2} [35, 104]. In contrast, in the nano-fretting tests only gradual changes in depth and friction were observed. To illustrate the relationship between friction and depth/wear rate Fig. 4(a) shows the friction coefficient and depth increase over the first 1000 cycles of a 3000 cycles test that didn't result in complete wearing through of the film. At the start of the test there is the suggestion of some blistering, presumably from debris generation in the contact. Optical microscopy of wear scars confirmed this debris was removed to edge of scar with continued cycling. Fig. 4(b) shows the relationship between friction and depth/wear rate in a 6000 cycles test where the film was completely removed. In this longer test there was an increase in wear rate after the depth increase reached ~70 nm (i.e. similar to film thickness).

3.4. Nano-scratch, micro-scratch, nano-fretting and reciprocating wear tests on DLC, Si-DLC, WC/C coatings on hardened M2 steel

The critical loads and friction coefficients at these transitions in scratch tests with 5 and 25 μm radius probes on DLC, Si-DLC, WC/C coatings on M2 steel are summarised in Table 5. Table 6 shows simulated von Mises stresses. In the nano-fretting and reciprocating wear tests the hard DLC coating showed the best wear resistance and the softer WC/C the worst. Fig. 5 (a-c) shows SEM images of the wear tracks in reciprocating tests at 500 mN. The Si-DLC shows more debris to the sides of the track than the other coatings. Fig. 5(d) shows the development in friction with continued cycles at 500 mN.

4. Discussion

4.1. Rate dependence on critical loads and friction

Table 3a shows that the scan speed dependence is small, so it is possible to compare results from different studies (e.g. with different probe geometries) where experimental conditions of loading and scan rates were not kept constant. This result is in agreement with data on ta-C [35] and DLC and Si-DLC on glass [105]. The critical load for failure of the 80 nm ta-C was almost constant (112 ± 9 mN) over a 100-fold variation in dL/dx [35]. Although slightly higher friction was associated with higher L_{c2} due to ploughing, over x100 difference in scan speed (0.1–10 μm/s) the mean friction coefficient at L_{c2} was 0.14 ± 0.01, as shown in Fig. 6. Similar results have been found at smaller contact size by AFM where friction forces between amorphous carbon and Si tips of radii 20–60 nm were almost invariant with scan speed over
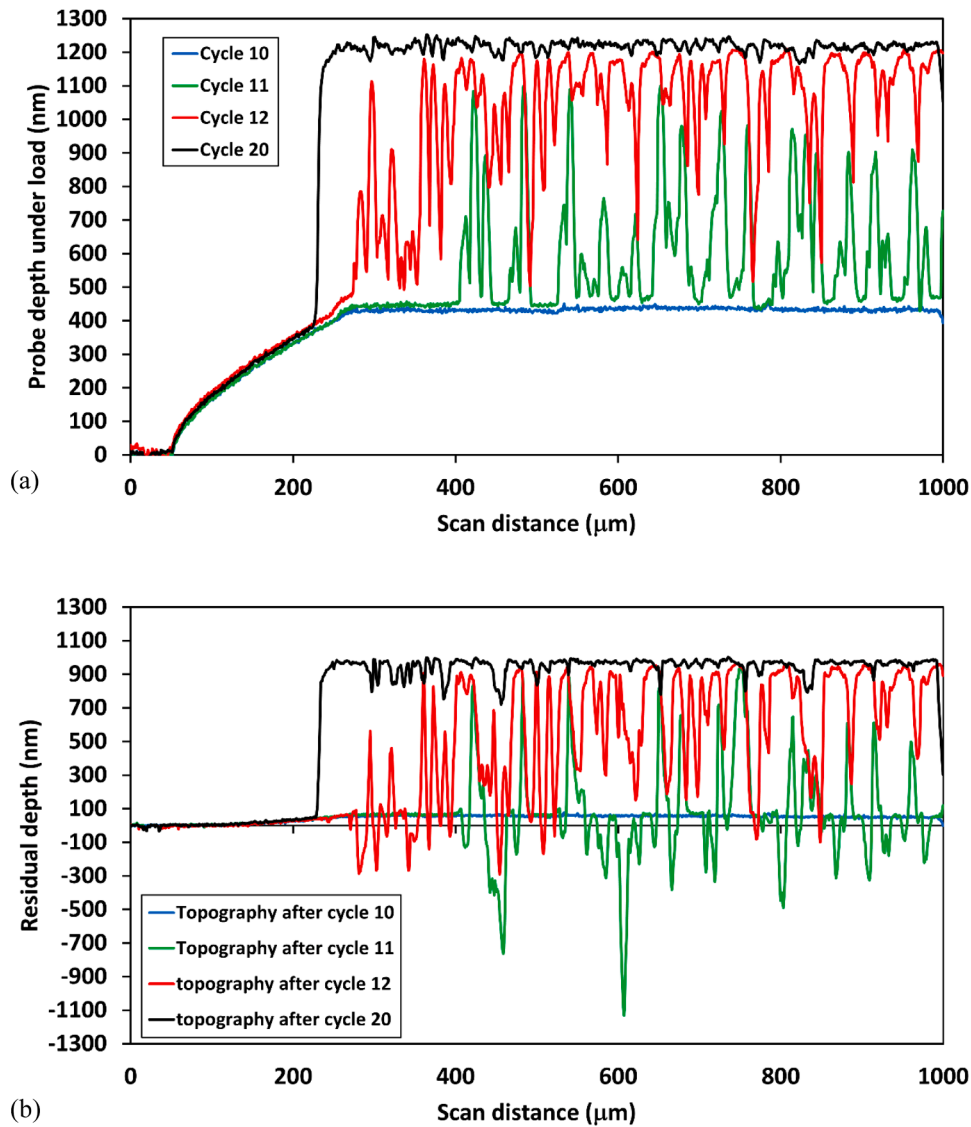
Fig. 1. Repetitive scratch test on 962 nm soft DLC at 70 mN; $R = 6.5$ μm. Selected cycles (a) probe depth under load (b) residual depth.

the range 0.1–2 μm/s [106].

4.2. Variation in scratch critical loads with probe sharpness

The indenter geometry calibration typically showed that the tip radius was not invariant, but its variation over the depth ranges reached in the scratch tests was sufficiently small that the probes could be assumed to be of constant radius for comparison purposes. Comparison of data in Tables 3(a-c) shows that the variation in critical loads with probe radius was much stronger for the thinner coatings on Si than the thicker DLC coatings on hardened tool steel. On the 80 nm ta-C the variation in L_{c1} with probe radius is shown in Fig. 7. This has been modelled by the dependence of the critical load being of the form

$$L_c = xR^m \tag{4}$$

Where m is a best fitting parameter. Assuming that yield (or cracking) occurs at a critical pressure, leads to the critical load depending on R^2. Contact mechanics analysis shows that for a flat surface in elastic/plastic contact with a rigid ball of radius R the yield pressure (P_y) is given by Eq. (5) [28,107].

$$P_y = 0.78R^2\left(H^3 / E^2\right) \tag{5}$$

For coating systems with different mechanical properties, thickness etc., the situation is more complex. For the thinnest film, 80 nm ta-C, the onset of yield is in the silicon substrate when using $R = 1.1$–9.0 μm probes and m~1.8. The calculated mean pressure (P_y) at yield was 12.0 GPa with R ~1.1 μm; 12.9 GPa with $R = 3.1$ μm; 14.8 GPa with $R = 4.6$ μm and 11.4 GPa with $R = 9.0$ μm. The mean pressures at yield were calculated using the same method specified in [36]. Utilising a spherical indenter, the contact depth (h_p) in an indentation contact is given by:

$$h_p = \frac{(h_t + h_r)}{2} \tag{6}$$

where h_p is the contact depth, h_t is the on-load scratch depth and h_r is the residual depth from the final scan. The contact radius (a) is determined by:

$$a = \sqrt{\left(2Rh_p - h_p^2\right)} \tag{7}$$

where R is the indenter radius. Finally, the contact pressure, P_m, can be calculated at any point along the scratch track by:

$$P_m = \frac{L}{\pi a^2} \tag{8}$$
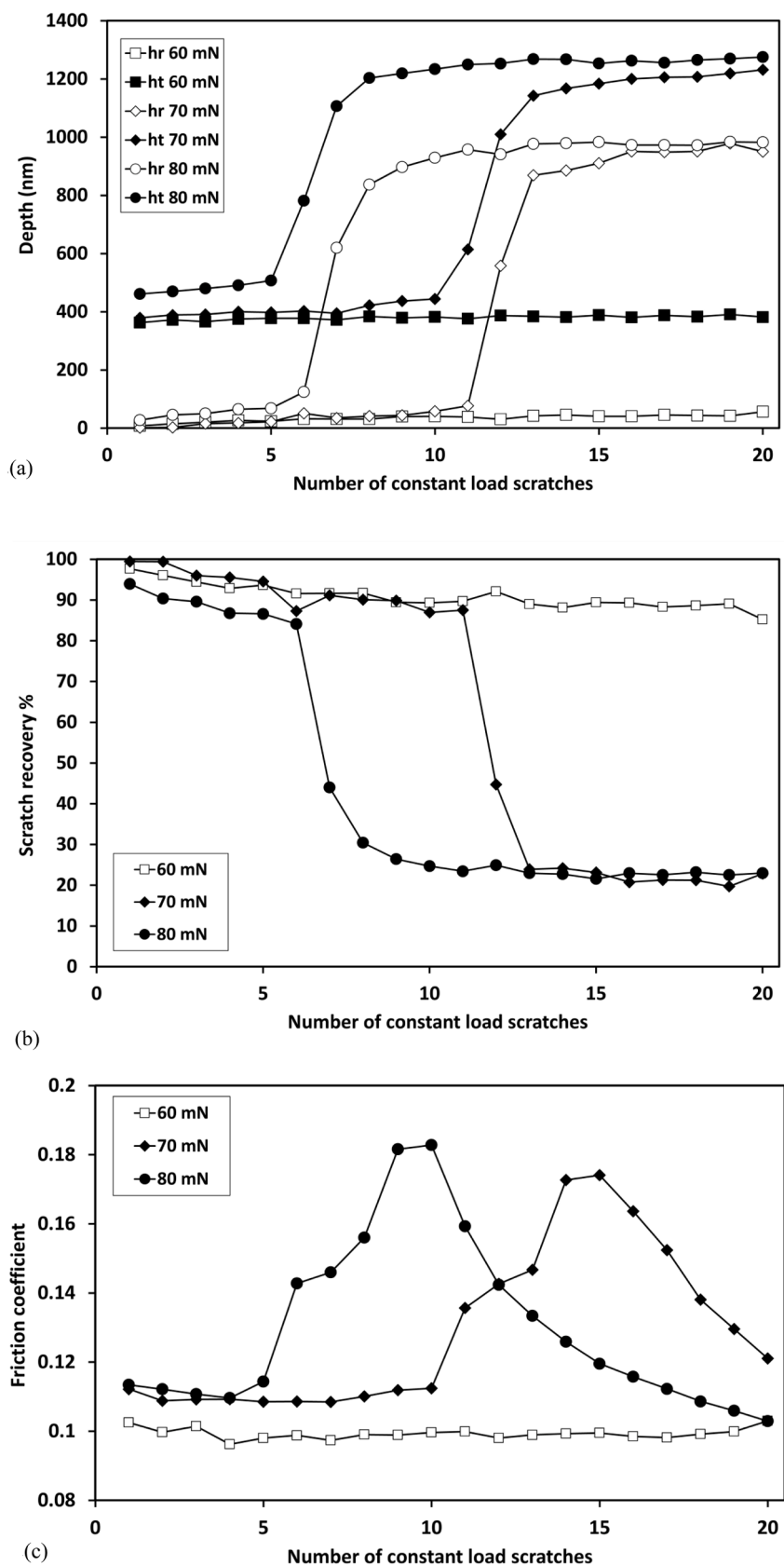
(a)

(b)

(c)

Fig. 2. Variation in (a) on-load depth and residual depth (b) scratch recovery (c) friction coefficient with continued cycles. Mean values averaged over entire constant load region.
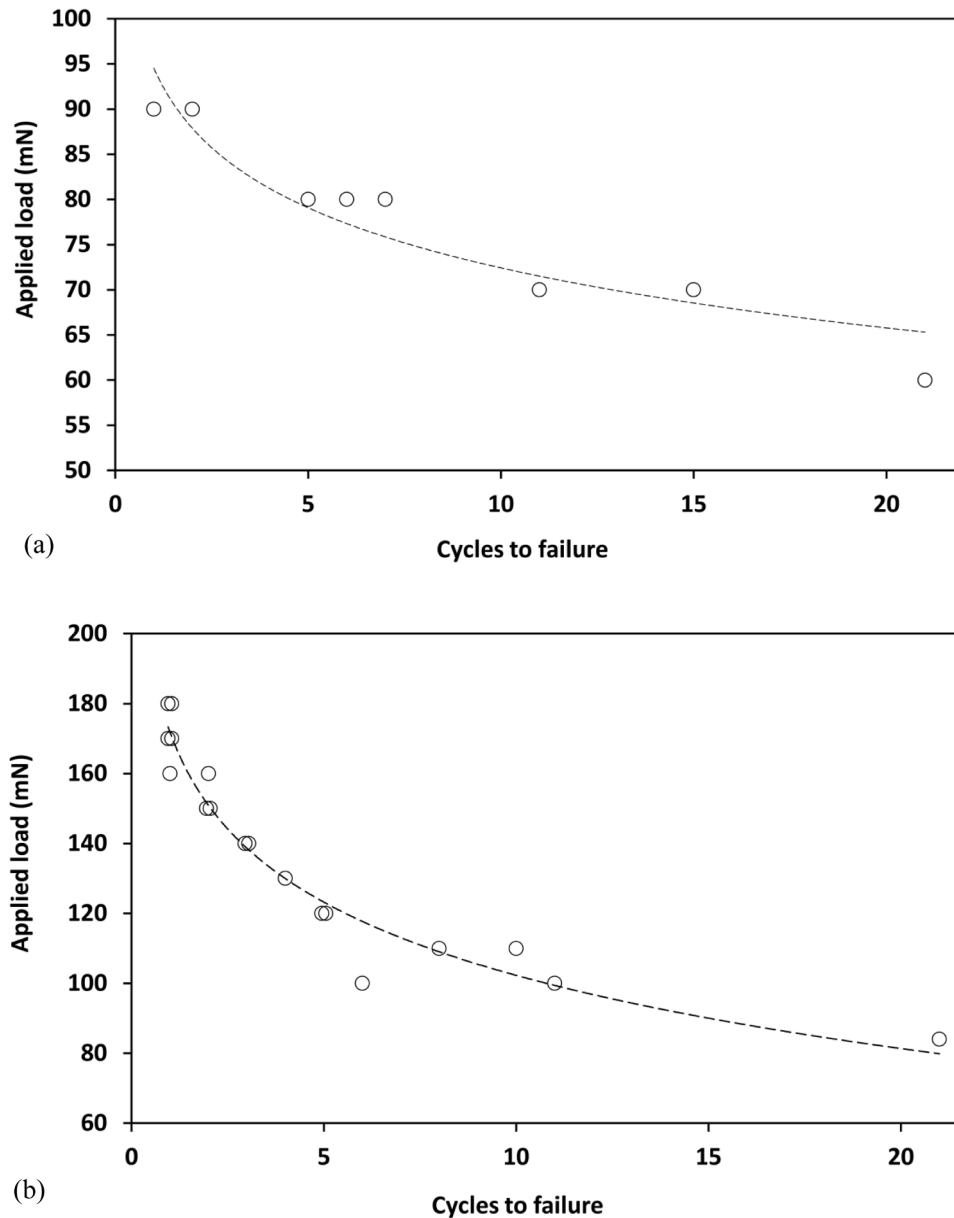
(a)

(b)

Fig. 3. Variation in number of cycles to failure for (a) 962 nm (b) 450 nm soft DLC. $R = 6.5$ μm. The lines are guides to the eye.

Table 4
Variation in critical load and friction with probe radius on 80 nm ta-C.

R (μm)	L_y (mN)	μ at L_y	L_{c1} (mN)	μ at L_{c1}	L_{c2} (mN)	μ at L_{c2}
1.1	1.7 ± 0.2	0.10	5.0 ± 0.6	0.17	7.5 ± 0.5	0.23
3.1	13.2 ± 0.7	*	35.7 ± 8.5	*	91.3 ± 3.8	*
4.6	52.8 ± 4.1	0.09	74.7 ± 5.5	0.12	$112.4 \pm 9.1§$	0.15
9.0	127 ± 18	*	182 ± 6	*	365 ± 16	*

Scan speed = 1 μm/s for 1.1 μm probe; 2 μm/s for others. *The frictional force was not recorded for the tests with 3.1 and 9.0 μm/s probes. § Some tests with this probe were continued to much higher load to determine the critical load for lateral cracking in the Si substrate, which was 276 ± 20 mN, with friction coefficient ~0.23.

where L is the applied load. At the onset of non-elastic deformation, $P_m = 1.1Y$. As yield stress of silicon is 11.3 GPa, so $1.1Y = 12.4$ GPa, which is almost the same as the pressure required for phase transformation (12 GPa) and hardness (12.5 GPa) emphasizing the importance of yield by phase transformation in the Si substrate [35,70]. Above this yield point Eq. (8) is not strictly exact as the load is then supported more on the front half of the sliding probe but nevertheless it can provide a reasonable estimate of contact pressure.

The coating systems displayed different behaviour how the scratch recovery at L_{c1} and L_{c2} varied with probe sharpness. On the ta-C film there was a slight decrease in scratch recovery with increasing probe radius and for the 450 and 962 nm soft DLC coatings the SR was higher for the larger probe. The extent of elastic recovery in an indentation test is correlated with the H/E ratio of the material being tested. SR is lower for the DLC, Si-DLC and WC/C coatings as the steel substrate has lower H/E than the Si. Rhee and co-workers reported that the deformation observed in indentation tests on bulk materials was dependant the radius of the indenter, with larger radii indenters (i.e. larger contact size) producing more brittle deformation and smaller radii indenters (i. e. small contact size) more plasticity [108]. In a sliding contact with tangential loading, in a bulk material scratch recovery will increase as contact size increases as plasticity is more important at smaller length
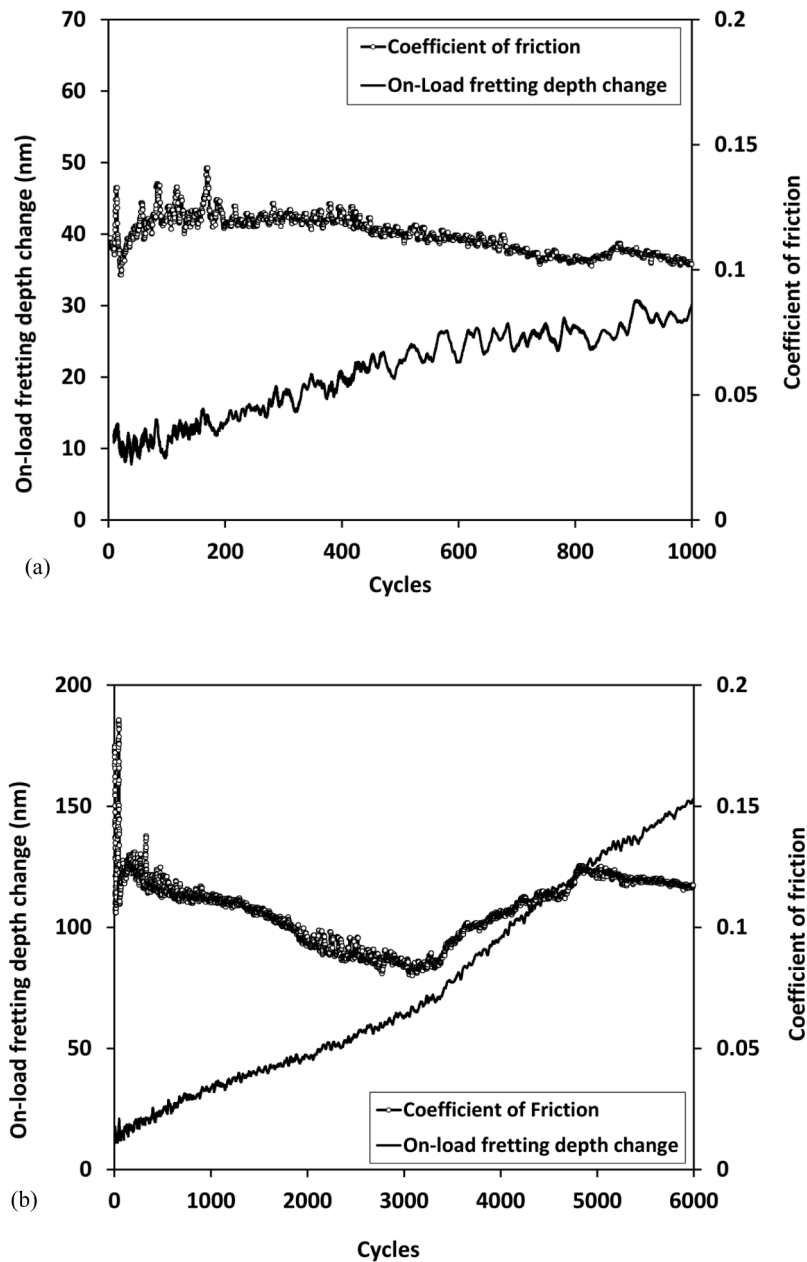
Fig. 4. Friction coefficient and depth changes in nano-fretting tests on ta-C at 200 mN with $R = 37$ μm. (a) initial 1000 cycles from a longer test (b) 6000 cycle test.

Table 5
dependence of critical loads and friction on probe radius for DLC, Si-DLC, WC/C in scratch tests with 5 and 25 μm radius probes.

Coating	R (μm)	L_y (mN)	μ at L_y	L_{c1} (mN)	μ at L_{c1}	L_{c2} (mN)	μ at L_{c2}
DLC	5	206 ± 5	0.115	422 ± 4	0.16	*	*
DLC	25	356 ± 9	0.075	2179 ± 120	0.175	2612 ± 127	0.195
Si-DLC	5	110 ± 10	0.117	445 ± 12	0.19	*	*
Si-DLC	25	383 ± 52	0.073	1827 ± 111	0.142	2256 ± 116	0.146
WC/C	5	68 ± 4	0.145	*	*	*	*
WC/C	25	375 ± 49	0.1	2830 ± 367	0.236	3695 ± 112	0.267

* L_{c1} or L_{c2} not reached before the maximum load (500 mN) in these tests was reached. Data previously reported in [13,125].

scales and fracture at larger scales. The relative proportion of deformation and fracture has a large influence on the subsequent wear in a tribological test and is an important factor in why coating hardness alone can be insufficient to predict wear rate.

4.3. Mechanistic differences in ramped load scratch tests on 450 and 962 nm soft DLC on Si

In the scratch tests with either the 3.7 or the 6.5 μm probes, the thinner soft DLC coating exhibited a slightly lower critical load for yield but greater critical loads for cracking and film failure. The nano-indentation results showed that the mechanical properties of these coatings were very similar so that the main differences in behaviour were due to their different thickness and how this influenced the stress fields developed. Higher L_y for the 962 nm soft DLC coating appears to be a consequence of the lower effective stiffness of the contact (rather than the coating alone) than for the 450 nm DLC, which therefore increased the resistance to plastic deformation (H^3/E^2) of the contact. In
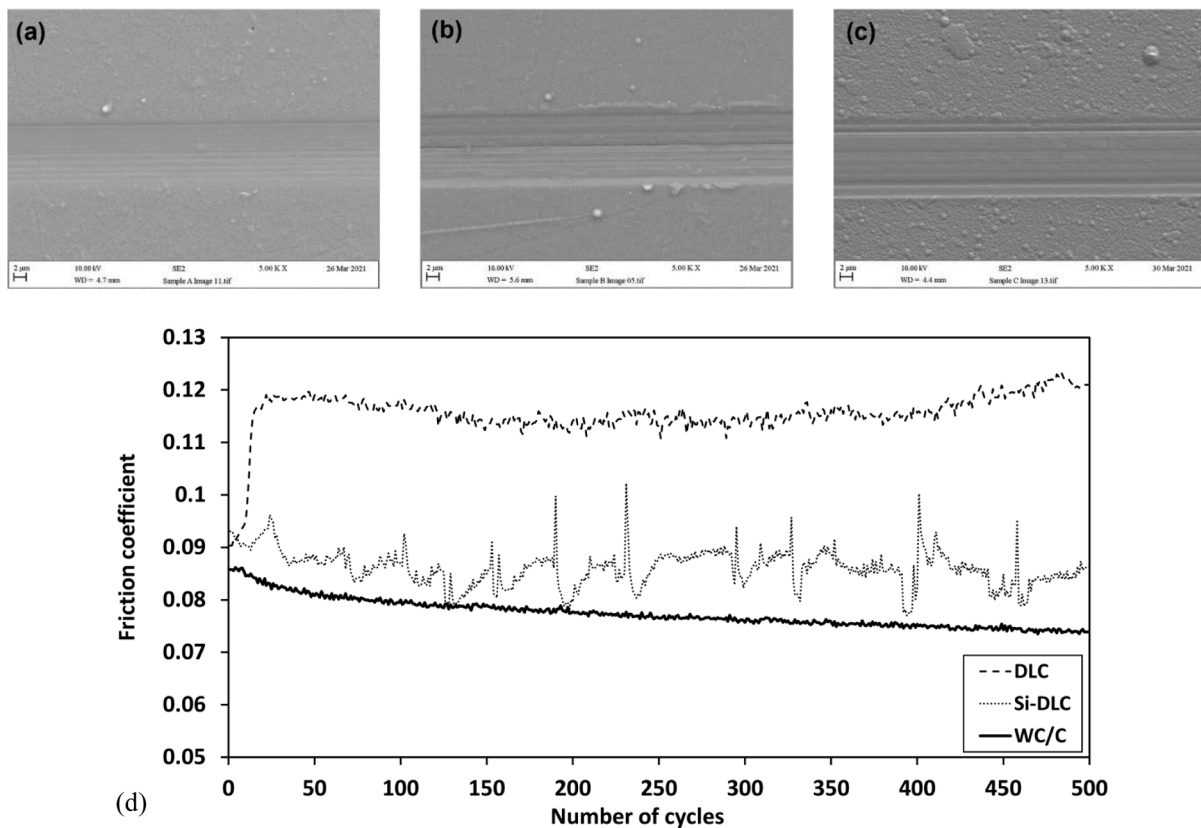
Fig. 5. SEM images of wear tracks after 500 cycles at 500 mN (a) DLC (b) Si-DLC (c) WC/C. $R = 25$ μm.
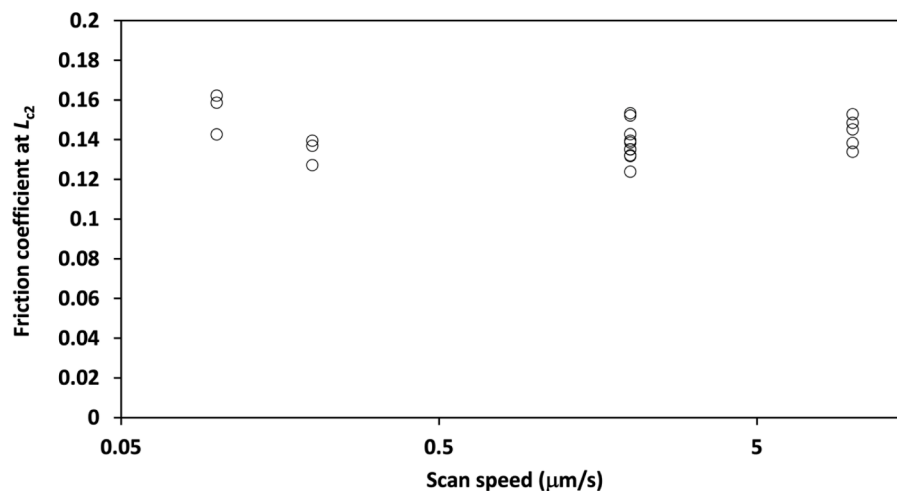
Fig. 6. Scan speed dependence on the friction coefficient at L_{c2}, 80 nm ta-C film, $R = 4.6$ μm.

comparison to the results on the harder coatings, the soft DLC yield at low P_m, as has also been reported for 70–150 nm soft MoST coatings on Si in scratch tests with a 3.1 μm probe [36]. Hertzian calculations suggest $P_m \sim 5.1$ GPa with the 3.7 μm probe and ~6.2 GPa with the 6.5 μm probe. Maximum von Mises stresses were located at ~315 nm below the surface with the 3.7 μm probe and ~540 nm below the surface with the 6.5 μm probe.

The greater load support provided by the harder and stiffer substrate will lower the bending stresses developed in the coatings at high load. SR (at failure) was higher for the thicker coating consistent with the greater proportion of the deformation being from the coating which has higher H/E than the Si substrate. There are differences in the developed

mean pressures at the onset of cracking for these coatings. Hertzian estimation shows that they were higher for the thinner coating, with maximum values located further below the surface. For the 450 nm DLC, the mean pressures were close to those required for phase transformation of the Si substrate, but they were lower for the 962 nm coating. Hertzian analysis indicated the maximum von Mises stresses were located within the substrate for the 450 nm coating and within the coating for the 962 nm coating. This difference may help explain why $(L_{c2}\text{-}L_{c1})$ is larger for the 962 nm coating since how the interface is weakened (from the coating side/interface side or both sides) has been shown to have a strong influence on coating failure in scratch tests [109, 110].
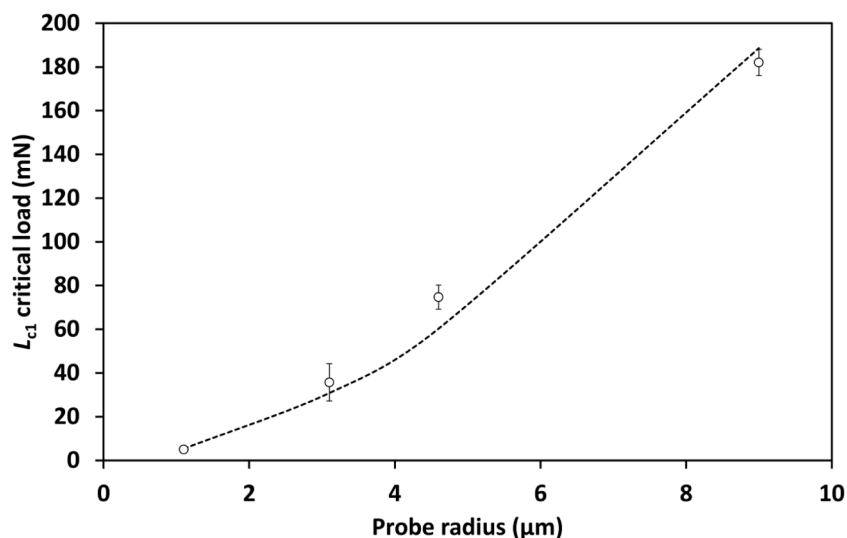
Fig. 7. Variation in L_{c1} with probe radius for 80 nm ta-C.

It is interesting to compare these soft DLCs with the behaviour of uncoated Si(100). In scratch tests at room temperature silicon displays brittle behaviour deforming by phase transformation and cracking [35, 70]. It has been shown previously that thin hard ta-C films were able to protect Si, increasing critical loads required for yield, cracking and lateral fracture [35,36,89]. Increasing film thickness improved their protective ability [35,36,89]. In contrast these soft DLCs exhibit much lower critical loads for yielding, but nevertheless offer some protection against cracking as they lower the stresses developed in the Si substrate, so that they can remain below that for phase transformation until higher load. For both probe geometries the critical pressures at L_{c1} were lower than needed for phase transformation for the thicker coating, indicating

(a)

(b)
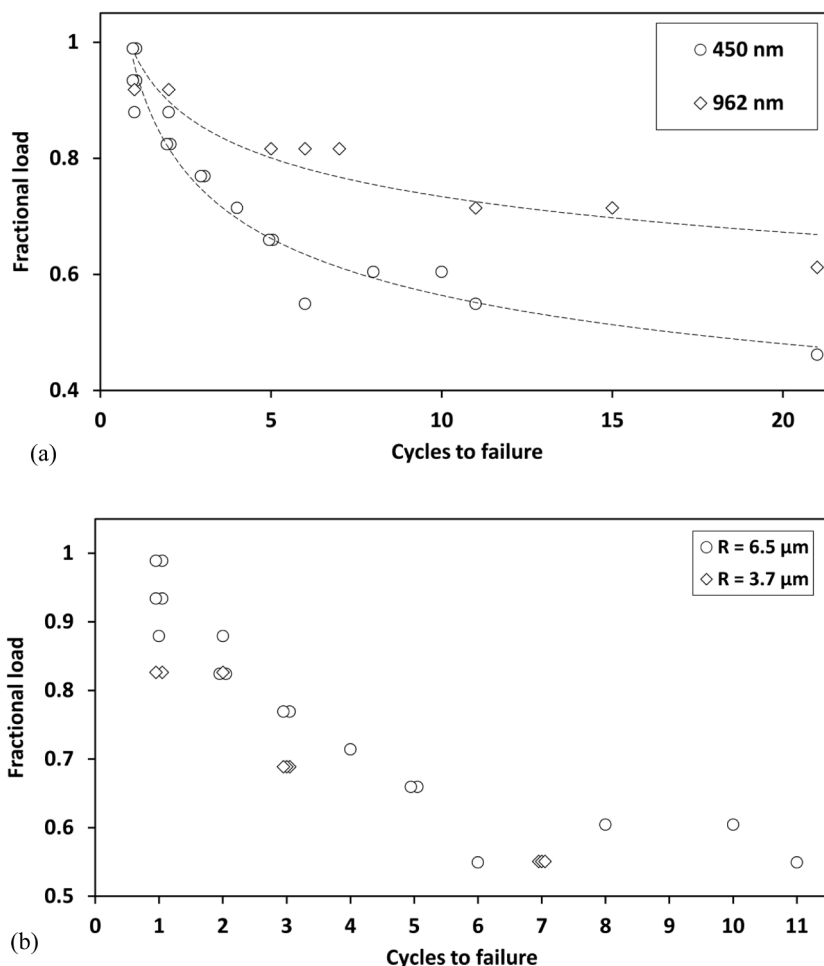
Fig. 8. Fractional load vs. cycles to failure (a) 962 nm and 450 nm with $R = 6.5$ μm (b) 3.7 and 6.5 μm on 450 nm soft DLC.

coating failure by an alternative mechanism.

4.4. Repetitive scratch test method development

The test methodology for assessing repetitive sub-critical constant load scratch tests has been developed enabling S-N type relationships to be determined. This approach is outlined in the recent CEN standard [97]. In tests where the load was close to L_{c1} the entire scratch track typically fails within 1–2 cycles of the onset of failure at a specific location but at lower load failure was more localised. Using the cycle-by-cycle evolution in the mean values (of h_t, h_t, SR, friction coefficient) from the entire track length under the constant repetitive load provided a convenient graphical method to follow the development of the failure process. The differences in L_{c2}-L_{c1} for the two soft DLC films discussed above influence their behaviour in the repetitive scratch test. Fig. 8(a) compares the number of cycles to failure vs. the fractional load (L/L_c) for these coatings. Under the sub-critical loads, the thicker coating shows relatively improved behaviour. This improved damage tolerance is consistent with the higher L_{c2}-L_{c1} found for this coating. In scratch tests on Si(100) with the same probe at 70–80 mN contact was almost elastic with low residual depth. Permanent deformation (i.e. wear) was predominantly of the coating explaining why the final residual depth in the repetitive scratch tests at these loads was close to coating thickness. In the repetitive scratch tests, the on-load depth at failure was lower than in ramped scratch tests. The difference was dependant on L/L_c and the film thickness. For the 450 nm DLC the depth at failure was much lower than for ramped tests. SR also decreased with each cycle. The differences between films were stronger than the probe

radius dependence. When normalised, the number of cycles to fail the 450 nm coating is similar for both probes (Fig. 8(b)), consistent with there being no change in failure mechanism over this range.

4.5. Contact size effects on critical loads

In studying wear mechanisms during repetitive scratching of steels with a 30 μm spheroconical tungsten carbide indenter, Kato and co-workers [111,112] observed that increasing load and contact strain resulted in a transition in wear mode from ploughing to wedge formation and then cutting at higher cone angles. To explain these changes in wear behaviour they introduced a degree of penetration parameter, D_p, defined as the on-load contact depth/contact radius, to characterise the severity of the abrasive contact. Coatings may experience greater bending stresses in scratch tests with sharper probes. In sliding contacts on coated systems Diao and co-workers proposed the ratio of coating thickness (t) divided by contact radius (a), t/a as an alternative severity index [113,114]. Finite element (FE) modelling showed that the magnitude of the tensile stresses generated at the rear of the contact was dependant on E_c/E_s and t/a [113,114]. The dependence of these two possible indicators of test severity, h_t/a and t/a, on test probe sharpness has been determined for the coatings systems studied. The contact radius (half contact width) a at yield can be determined from Hertzian analysis. Since elastic recovery is high for coating systems with high H/E an estimate of a can be determined at L_{c1} and L_{c2}. For all the coatings the values of t/a at the critical loads increased with decreasing probe radius. This can be most clearly shown in data on the ta-C coating where t/a at L_y increased from 0.046 with the 9.0 μm probe to 0.35 with the 1.1 μm

(a)

(b)
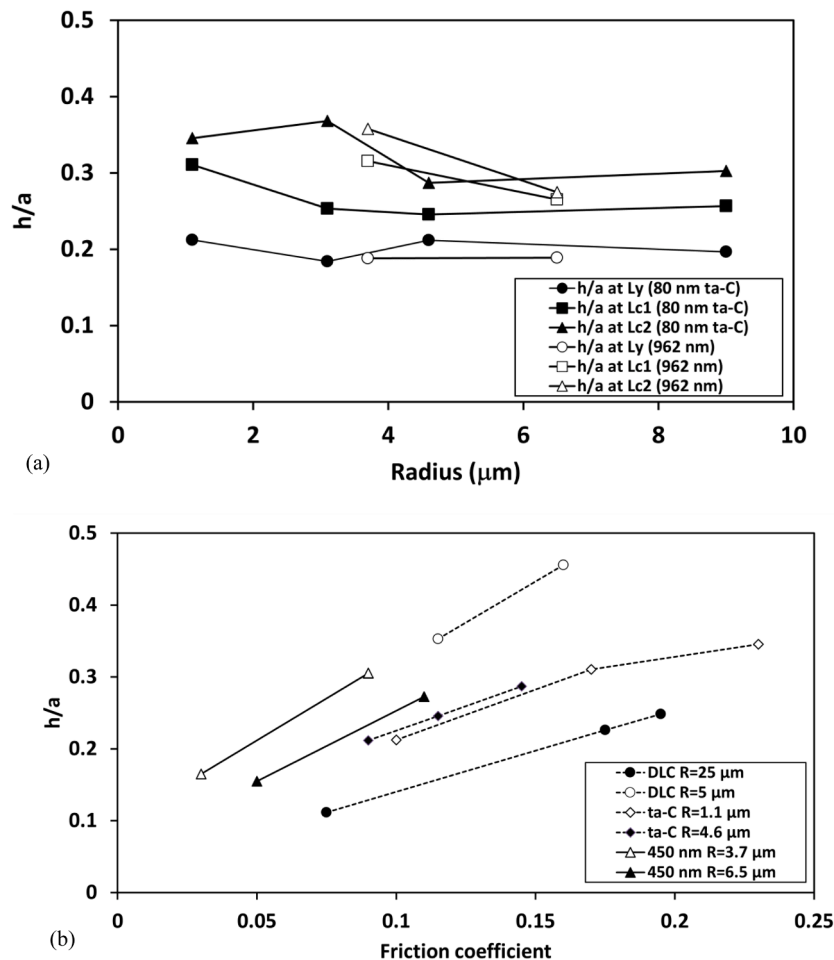
Fig. 9. Variation in h_t/a at the critical loads on (a) probe radius and (b) friction coefficient.

probe. The dependence of h_t/a at the critical loads on probe radius and friction coefficient is shown in Fig. 9(a) and 9(b) respectively. For the coatings on hardened tool steel h_t/a at critical load decreased with increasing probe radius but this parameter was less influenced by probe radius for the ta-C and soft DLC coatings on silicon, with L_y being approximately constant, though a slight trend remained for L_{c1} and L_{c2}.

The friction coefficient at yield is not constant as different ploughing contributions are observed depending on probe sharpness (Fig. 9(b)). Higher friction from increased ploughing is observed when there is appreciable plasticity prior to failure, e.g. as on DLC, Si-DLC and WC/C on M2 steel (as discussed below) and where increasing depth causes a change in probe attack angle and/or reduction in effective tip radius.
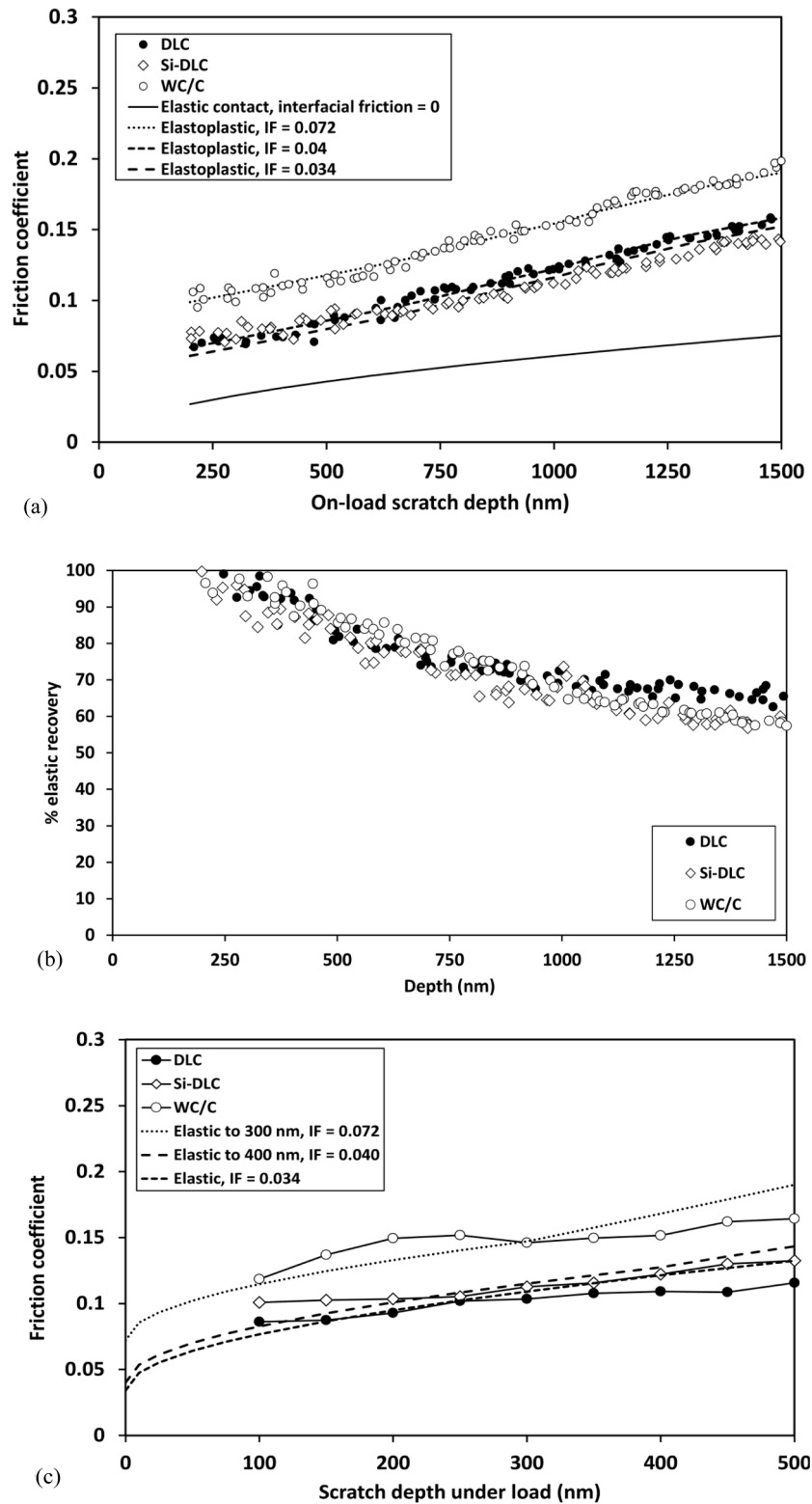
Fig. 10. (a) Friction vs. on-load depth for scratch tests on DLC, Si-DLC and WC/C, $R = 25$ μm (b) scratch recovery with $R = 25$ μm (c) scratch tests on DLC, Si-DLC and WC/C $R = 5$ μm.

This appears to be the case for the tests on the ta-C with R ~1.1 μm.

4.6. Ploughing and friction

Several authors have attempted to deconvolute the interfacial and ploughing components in the Bowden and Tabor model [88,115–117].

$$\mu_p \approx q \frac{\left(R^2 \cos^{-1}\left(\frac{(R-h)}{R}\right) - (R-h)\sqrt{h(2R-h)}\right)}{\left(\pi\left(2Rh - h^2\right)\right)} \quad (9)$$

The ploughing term has been determined from the geometrical comparison of normal and lateral contact areas. In the limit of fully plastic scratching with no recovery $q = 2$ but this is not achieved in these tests with spherical probes. In the fully elastic regime, the load is equally supported on front and back ½ of the sliding probe ($q = 1$). From calculating the ploughing component in the elastic regime and comparing to measured friction the difference should be the interfacial component. The measured friction will rise more rapidly with increasing scratch depth once there is non-elastic behaviour as the load is less supported on the back ½ of the sliding contact.

The importance of elastic recovery on friction has been highlighted by Lafaye and Troyon [118] to explain bilinear friction vs. load behaviour in AFM nano-scratch tests on Cu, Ti6Al4V and Al. By simulating the degree of elastic recovery through a varying rear angle they were able to more accurately fit the experimental AFM friction data. In the current work the friction model has been modified to account for differences in elastic recovery by allowing q to be a fitting parameter that varies with depth. Since the on-load and residual depths were measured in our tests it is possible to determine the depth-dependence in scratch recovery and use this in obtaining a better fit to the experimental nano- and micro- scale scratch friction data. Scratch tests on uncoated Si (100) with the 6.5 μm probe and scratch tests on the DLCs on M2 steel with the 25 μm probe, clearly show increased friction at the onset of non-elastic behaviour.

In the model, a constant probe radius has been assumed for simplicity and surface topography has been neglected. Fig. 10(a) shows results for the DLC, Si-DLC and WC/C with the 25 μm probe. Fitting parameters are the interfacial friction, determined from best fit in the elastic regime and the q parameter which gradually increased from 1 to 2 in accordance with the experimental scratch recovery data (Fig. 10 (b)). This approach could closely replicate the more rapid increase in friction from the onset of non-elastic deformation. The frictional data at low penetration depth show some variability due to the higher geometrical influence of the surface topography as discussed by Achanta

and co-workers [71–73], so the fitting was performed over a range of on-load depths that were high enough to minimise topographic influence but below L_{c1}. Pagnoux and co-workers have estimated the contact boundary in scratch tests with 50–200 μm diamond probes on a similar multilayered Si-DLC coating (2.5 μm (a-C:H + Si:a-C:H)/0.9 μm CrN + Cr on M2 steel) [119]. Their data suggests that the contact is a little more than half supported on the rear of the probe. This is close to our fitting value rising to 1.57. SR is 100% to ~300 nm ($q = 1$) and then decreases to ~65% at 1500 nm ($q = 1.57$).

The interfacial friction coefficients vs. diamond were estimated as 0.072 for WC/C, 0.040 for Si-DLC and 0.034 for DLC. These values of interfacial friction were combined with the experimental SR data from the $R = 5$ μm probe to fit the friction vs. depth data with this probe (Fig. 10(c)). With the sharper probe the SR differed between the samples due to their different mechanical properties (e.g. H/E and H^3/E^2). Deformation was elastic over this range on the DLC, with non-elastic behaviour above 400 nm for Si-DLC and 300 nm for WC/C. The fit is not perfect but nevertheless encouraging. As a further test of the potential robustness of the method it was applied to fitting the friction vs. depth data of the thicker soft DLC with the 6.5 μm probe (Fig. 11). Deformation is very close to elastic on this coating up to 400 nm so the data was fitted with $q = 1$ over this depth range. The behaviour was contrasted to scratch tests on uncoated Si(100) with the same probe where there was a more rapid rise in friction coefficient from ~200 nm. The on-load and residual depth data in Fig. 12 show that this is consistent with the onset of plasticity/fracture at this point.

4.7. Friction and wear mechanisms in the different tribological tests

The contact pressures are typically higher in ramped scratch tests and lower in repetitive tests at lower load, although they can still be relatively high. This can result in the dominant deformation mechanisms changing in the different types of test. Failure is by relatively large-scale cracking with abrupt events in nano-scratch (high compressive stresses, tensile stresses etc.). In contrast, there is a transition to micro-wear in fretting tests where the coating is gradually worn away, as shown in Fig. 4b. Similar behaviour has also been reported in lower load nano-fretting tests on 5 and 20 nm ta-C films where EDX profiles show coating thickness reduction and oxygen incorporation in the wear track (i.e. a tribo-oxidation component for these thin films that was absent on the 80 nm ta-C) [35].

There was a correlation in coating performance between the 4500 cycles fretting and ramped nano-scratch test results on the 80 nm ta-C despite the differences in contact pressure and failure mechanism in

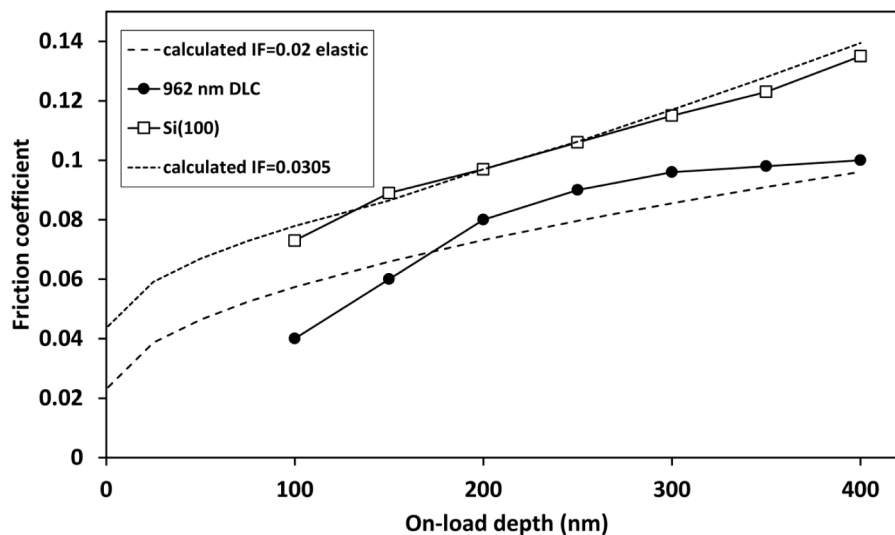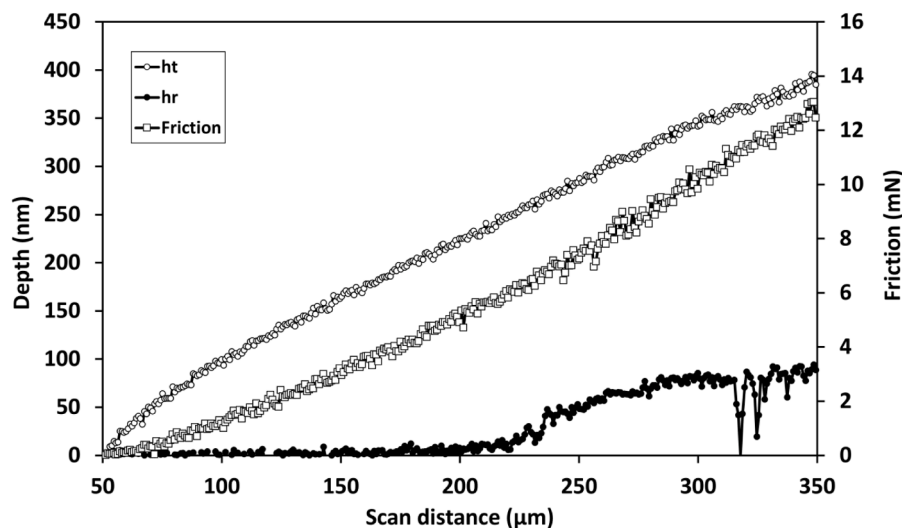**Fig. 11.** Friction vs. on-load depth for 962 nm and Si(100) with $R = 6.5$ μm.

Fig. 12. Ramped load scratch test on Si(100) with $R = 6.5$ μm.

the tests. This 80 nm film provided more load support and protection of the Si substrate than thinner films. Thinner films offered significantly less protection, failing at lower load in the scratch test and more rapidly and/or at lower load in the fretting test. Chen and co-workers studied AFM nano-wear of 2 and 5 nm DLC films deposited by filtered cathodic arc on Si(100) against $R = 1$ μm SiO_2 and $R = 0.5$ μm diamond tips [68]. Although the thicker DLC showed the best wear resistance the thinner film also was more wear resistant than the Si(100). Interestingly, Wilson and co-workers reported in high cycle (to 216,000 cycles) nano-fretting tests of 10–2000 nm sputtered Cr doped amorphous C films with a ruby sphere of radius 150 μm the specific wear rate reduced exponentially with decreasing film thickness [67,120–122]. Greater wear for the thicker films may relate to them being more stressed than the thinner films or simply that the coatings were significantly less resistant to fretting wear than the Si substrate as the mean contact pressure in these tests (at low load and with large radius probe) was much lower than the phase transformation pressure so that the substrate did not wear at all.

4.8. Variation in friction with continued wear cycles

In the absence of film failure, the friction force in a repetitive scratch test tends to gradually decrease with each cycle due to a progressive reduction in ploughing component. In addition to hard coatings this type of behaviour has been observed in several materials besides coatings, including bulk metallic alloys such as 316 L stainless steel, CoCr [123] and copper [103], the major exception is when sliding breaks up a passive protective oxide resulting in severe wear and continuing high friction, e.g. on Ti6Al4V. Korres and co-workers [124] developed a geometric model correlating wear track widening and friction which assumed no elastic recovery. Interestingly, although the contact approaches conformal with continued cycles it was still possible to correlate the friction with changing ploughing via changes to the track width. When there is little change in depth with cycles, as e.g. in the test at 60 mN in Fig. 2(c), the friction coefficient did not change significantly, remaining near to 0.1. However, the SR is changing slightly, indicating some micro-scale cracking and/or densification, so the Korres model potentially might be a slight over-simplification, at least for the first few cycles of a repetitive test.

The relationship between evolving friction and cycling is more complex when failure occurs and/or wear becomes important. After initial reduction in ploughing component over a few cycles, subsequent frictional changes are due to a combination of factors including (i) changing contact area (ii) formation of transfer layers (iii) third body effects (iv) changing probe geometry (e.g. moving from spherical end to

conical part of the probe as penetration depth increases). At coating failure (e.g. from cycle 11 at 70 mN in Fig. 2(c)) there is an increase in mean friction and subsequent decrease as damaged material is ploughed out of the scratch track.

In nano-fretting and reciprocating tests various types of responses were typically observed including (i) a gradual initial increase in friction followed by subsequent reduction – e.g. for DLC on M2 in fretting and reciprocating sliding (ii) initial variability then reduction and subsequent increase – e.g. for ta-C on Si. To an extent friction and wear rate are correlated, higher friction after failure could partly relate to changing interfacial component since the interfacial friction between Si and diamond is higher (e.g. see Fig. 11). Wang and co-workers have reported that in ambient conditions in 2000 cycles of AFM sliding between a $R = 100$ nm Si tip and DLC the friction coefficient gradually decreased from 0.17 to 0.16 [53]. Larger changes were observed in UHV conditions and the authors proposed oxide layer breakage as responsible and suggested that under ambient conditions it might be continually being broken and reformed.

4.9. Influence of mechanical properties

In the tests on the DLC, Si-DLC and WC/C coatings on M2 steel the radius of the scratch probe strongly influenced the yield behaviour. Correlation between coating properties and critical load for yield was found with the sharper probe but not with the larger radius probe [13, 125]. Simulations of the stress distributions generated in the scratch tests have been performed. These were able to explain how the coating mechanical properties influence the behaviour differently when changing the probe sharpness, and result in different trends in L_y and L_{c1}. The developed von Mises stresses were compared to the yield stress at that point to determine a local yield map, as has been done by Diao and Kato [113] using FE. In scratch tests with the $R = 5$ μm indenter the initial yield occurred within coating for the WC/C and Si-DLC but in the substrate for the much harder DLC coating [98]. Table 5(a) shows that the von Mises stresses developed in the coatings, especially the DLC coating system, were extremely high. With increasing load, the yielding location moved into the steel substrate, which was over-stressed from the coating-substrate interface, for all three coatings. The resistance to cracking (L_{c1}) correlated with coating mechanical properties. In the ramped load tests to 500 mN with the $R = 5$ μm indenter, the cracking present on the DLC and Si-DLC coatings was not observed on the softer, lower H/E WC/C coating [13]. More extensive yielding on this coating may have acted as a source of stress relaxation reducing the driving force for cracking. In the scratch test the shear stress distribution is

asymmetric with maximum compressive stress in front of the probe and a maximum tensile stress behind which results in cracking when it exceeds the fracture strength of the coating [126–129]. Peak tensile stresses at the rear of the sliding contact were in the region of 5–7 GPa [98]. With the $R = 25$ μm probe yield began in the substrate, resulting in similar L_y and corresponding on-load scratch depths on all three coatings. The results of the simulations are consistent with coating failure occurring through a combination of high tensile stress with plastic flow in the substrate adjacent to the coating-substrate interface, as has been suggested previously for hard coatings on cemented carbide [130].

Table 6a

Table 6a
Maximum von Mises stresses with $R = 5$ μm.

| | Maximum von Mises stress (GPa) | | | |
	in coating at L_y	in substrate at L_y	in coating at L_{c1}	in substrate at L_{c1}
DLC	20.6	5.1	8.7	5.2
Si-DLC	13.8	3.2	7.2	5.0
WC/C	11.2	3.2	7.4	5.2

Table 6b

Table 6b
Maximum von Mises stresses with $R = 25$ μm.

| | Maximum von Mises stress (GPa) | | | |
	in coating at L_{c1}	in substrate at L_{c1}	in coating at L_{c2}	in substrate at L_{c2}
DLC	6.5	5.2	6.5	5.2
Si-DLC	6.7	5.1	6.6	5.2
WC/C	6.8	5.5	7.3	5.6

The relative wear resistance of the three coatings was dependant on the type and severity of the test and the contact length scale as controlled by the applied load and test probe radius as the optimum coating mechanical properties (balance of load support and fracture resistance) vary with the test. The WC/C performed best in terms of higher L_{c1} and L_{c2} in the scratch tests but in the nano-fretting and reciprocating tests the coating ranking changed, with the hardest coating showing the highest wear resistance and WC/C the least. In the reciprocating and nano-fretting tests the initial contact pressures were ~11–14 GPa, gradually decreasing with continued cycling through wear. On the ta-C the initial pressures in the nano-fretting tests are lower. Material removal appears to be through a combination of fatigue (micro) wear and plastic deformation.

The nano-fretting and reciprocating tests were performed at loads well below those causing cracking in ramped scratch tests (i.e. (i) 4500 cycles at 100 mN with $R = 5$ μm; $L_{c1} >420$ mN, $L/L_c <0.24$; (ii) 500 cycles at 10–500 mN with $R = 25$ μm; $L_{c1} >1800$ mN, $L/L_c <0.28$). With continued cycling crack formation is possible below L_c due to low cycle fatigue. Schiffmann noted that periodic loading in reciprocating sliding leads to an accumulation of plastic deformation and/or densification of the material that gradually increases the subsurface stress in the coating [131,132], resulting in formation of micro-cracks. The increase in wear depth is a combination of material removal and plastic deformation [131,133]. At nano/micro-scale plastic deformation is a major contributor to apparent wear. In the nano-fretting and reciprocating tests at low L/L_c and high t/a (i.e. small scratch depths) the tensile stresses were much lower than at higher loads and coating wear resistance was largely controlled by the coatings resistance to plastic deformation (i.e. hardness). In reciprocating tests with a $R = 1$ μm diamond, Gee et al. also reported lower wear resistance for WC/C than for harder DLC coatings

[134]. As the test severity increases t/a reduces and tensile stresses become important, and wear is more influenced by micro-cracking. SEM imaging of wear tracks show grooving wear and debris to the sides of the track on Si-DLC which had the lowest L_{c1} in scratch tests with same $R = 25$ μm geometry probe.

4.10. Friction and contact area/topography

The onset of variability in friction force observed at coating failure is primarily due to instantaneous changes in contact area. Santner and coworkers have studied the interdependence of friction and surface topography describing the geometric changes in friction where sliding probes encounter topographic features [57–60]. They reported a sharp reduction in friction when sliding down an asperity/step and a sharp increase when sliding up an asperity/step. This was explained by changing contact area. When encountering a step there is a greater contact area due to the additional contact in front. On encountering a recessed region the contact area decreases and there is a reduction in friction. Since the effect was present in oil and in air [57] adhesion was not considered responsible [60].

This effect can also be clearly seen in the ramped and repetitive scratch tests. Fig. 13 shows typical examples for the 962 nm soft DLC. In this case the surface topography is being created by the scratch itself but the frictional behaviour appears to be exactly the same. In Fig. 13 (a-c) the surface profiles are inverted, i.e. probe depth (to be consistent with how they are shown in nano-scratch tests [97]) rather than height is shown. The abrupt change in friction with a reduction at first failure is due to an abrupt decrease in contact area.

However, in the nano-fretting tests on ta-C shown in Fig. 4, friction and wear rate are correlated which appears to be a contact area effect. Effects including a transfer film formation and/or breaking/reforming < 1 nm native oxide layer may also play a role [52,53]. The adhesion term dominates friction when there is high surface conformity and friction scales with contact area [135]. The on-load and residual depth data enable contact area to be estimated. Abrupt and gradual changes in probe depth have different influences on the contact area and hence the adhesion contribution to the measured frictional force. Typically, a gradual increase in depth is due to material removal that gradually increases the area in contact, whereas an abrupt increase in probe depth is associated with a (transitory) decrease in contact area due to fracture.

In the reciprocating tests on the DLC, Si-DLC and WC/C the local surface topography in the wear track influenced the mean friction coefficient at low load, although as the load was increased its influence rapidly decreased. In AFM friction measurements more variability in friction has been reported than in tests with higher loads and blunter probes [71–73]. In the lowest load in the reciprocating tests 10 mN there was a small increase in friction over the initial ~50 cycles, which was suggested [125] to be a surface topographical effect through increasing contact area (asperity polishing), together with difficulty in forming a transfer layer in light contact on rough surfaces [136]. At higher load changes in friction during the first few cycles were related to increasing contact area as asperities break down. Similar behaviour was reported in fretting testing of a hard DLC coating against silicon nitride under gross slip conditions [73].

SEM images of wear tracks on the DLC, Si-DLC and WC/C show differences that relate to relative proportion of micro-cracking and friction. Si-DLC shows no reduction in friction with continued cycling at ≥ 300 mN, grooving in the wear track and more debris on the side of the track. Friction on DLC was consistent with ploughing/transfer film formation at 50–200 mN with a transition to higher friction at 500 mN. Friction on WC/C at ≥ 100 mN tended to decrease with cycles at higher load. In comparison, the nano-fretting tests on ta-C showed frictional changes with cycling consistent with a gradually increasing contact area, with debris working out of the contact.
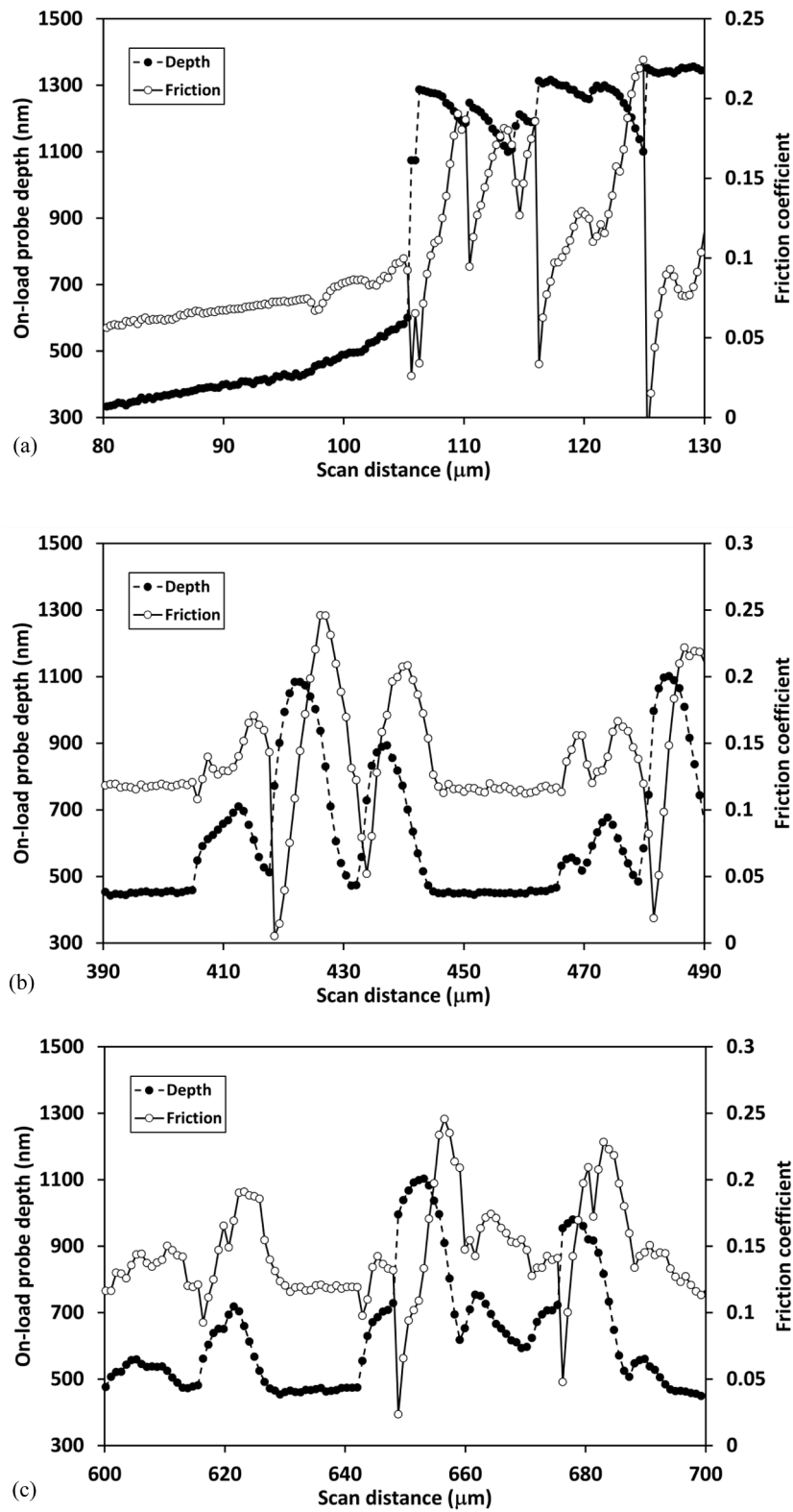
Fig. 13. Relationship between friction coefficient and probe depth in tests on 962 nm soft DLC with *R* = 6.5 μm over (a) the 50 μm region of the track around failure in a ramped load scratch test (b,c) over 2 different 100 μm regions of the wear track in the cycle that failed in a constant load repetitive scratch test (cycle 11 in a test at 70 mN in this case).

5. Conclusions

Contact size and mechanical properties influence the friction and wear of DLC in scratch and reciprocating tests with diamond probes. In scratch tests the critical loads and friction coefficients at failure were relatively insensitive to changing loading conditions and scan speed. This enables results of tests with different loading conditions to be compared so that effect of probe sharpness can be assessed quantitatively.

Friction was influenced by ploughing in ramped scratch tests, repetitive contact scratch tests and reciprocating tests through evolving contact area. This results in, for example, different friction coefficients at the onset of yield when different probe geometries are used.

Scratch tests on uncoated silicon with a $R = 6.5$ μm probe and on DLCs with a $R = 25$ μm probe clearly show increased friction coefficient at the onset of non-elastic behaviour. A 2-term friction model has been modified to account for differences in elastic recovery. Since the on-load and residual depths were monitored in the scratch tests it was possible to determine the depth-dependence of the scratch recovery and use this as a variable parameter in obtaining a better fit to the experimental nano-/micro- scale scratch friction data.

A test methodology for assessing repetitive sub-critical constant load scratch tests has been developed. The repetitive scratch test has elements of a low-cycle fatigue test where S-N type relationships can be determined.

Mechanical properties influence the evolution in friction and wear through e.g. yield location.

The influence of surface topography on friction has been shown in ramped and constant load scratch tests. When fracture occurred resulting in a sudden increase in probe depth there was an abrupt decrease in friction which is ascribed to a contact area effect. In contrast, where deformation progressed through micro-wear a more gradual increase in depth can be associated with higher contact area and higher friction.

Declaration of Competing Interests

The authors declare that they have no known competing financial interests or personal relationships that could have appeared to influence the work reported in this paper.

Acknowledgments

References

[1] J. Robertson, Diamond-like amorphous carbon, Mater. Sci. Eng. R Reports. 37 (2002) 129–281, https://doi.org/10.1016/S0927-796X(02)00005-0.

[2] H.O. Pierson, Handbook of Carbon, Graphite. Diamonds and Fullerenes: Processing, Properties and Applications (Materials Science and Process Technology), Noyes Publications, 1993, https://doi.org/10.1016/B978-0-8155-1339-1.50008-6 doi:https://doi.org/.

[3] J. Robertson, The deposition mechanism of diamond-like a-C and a-C: H, Diam. Relat. Mater. 3 (1994) 361–368, https://doi.org/10.1016/0925-9635(94)90186-4.

[4] A. Ferrari, J. Robertson, Interpretation of Raman spectra of disordered and amorphous carbon, Phys. Rev. B - Condens. Matter Mater. Phys. 61 (2000) 14095–14107, https://doi.org/10.1103/PhysRevB.61.14095.

[5] A. Erdemir, The role of hydrogen in tribological properties of diamond-like carbon films, Surf. Coatings Technol. 146–147 (2001) 292–297, https://doi.org/10.1016/S0257-8972(01)01417-7.

[6] A.C. Ferrari, J. Robertson, Resonant Raman spectroscopy of disordered, amorphous, and diamondlike carbon, Phys. Rev. B - Condens. Matter Mater. Phys. 64 (2001), 075414, https://doi.org/10.1103/PhysRevB.64.075414.

[7] J.C. Angus, Empirical categorization and naming of "diamond-like" carbon films, Thin Solid Films 142 (1986) 145–151, https://doi.org/10.1016/0040-6090(86)90310-X.

[8] S.V. Hainsworth, N.J. Uhure, Diamond like carbon coatings for tribology: production techniques, characterisation methods and applications, Int. Mater. Rev. 52 (2007) 153–174, https://doi.org/10.1179/174328007x160272.

[9] M. Zhong, C. Zhang, J. Luo, Effect of substrate morphology on the roughness evolution of ultra thin DLC films, Appl. Surf. Sci. 254 (2008) 6742–6748, https://doi.org/10.1016/j.apsusc.2008.04.059.

[10] J.C. Sánchez-López, A. Fernández, Doping and alloying effects on DLC coatings, Tribol. Diamond-Like Carbon Film. Fundam. Appl. (2008) 311–328, https://doi.org/10.1007/978-0-387-49891-1_12. Springer US, Boston, MA.

[11] J. Zheng, H. Zhou, Z.H. Wan, R.P. Sang, Structure and mechanical properties of tungsten-containing hydrogenated diamond like carbon coatings for space applications, Phys. Procedia, Elsevier B.V. (2011) 245–250, https://doi.org/10.1016/j.phpro.2011.06.089.

[12] X. Chen, Z. Peng, Z. Fu, S. Wu, W. Yue, C. Wang, Microstructural, mechanical and tribological properties of tungsten-gradually doped diamond-like carbon films with functionally graded interlayers, Surf. Coatings Technol. 205 (2011) 3631–3638, https://doi.org/10.1016/j.surfcoat.2011.01.004.

[13] B.D. Beake, T.W. Liskiewicz, V.M. Vishnyakov, M.I. Davies, Development of DLC coating architectures for demanding functional surface applications through nano- and micro-mechanical testing, Surf. Coatings Technol. 284 (2015) 334–343, https://doi.org/10.1016/j.surfcoat.2015.05.050.

[14] Q. Yong, G. Ma, H. Wang, S. Chen, B. Xu, Influence of tungsten content on microstructure and properties of tungsten-doped graphite-like carbon films, J. Mater. Res. 31 (2016) 3766–3776, https://doi.org/10.1557/jmr.2016.433.

[15] J.L. Lanigan, C. Wang, A. Morina, A. Neville, Repressing oxidative wear within Si doped DLCs, Tribol. Int. 93 (2016) 651–659, https://doi.org/10.1016/j.triboint.2014.11.004.

[16] B.J. Rodriguez, T.L. Schiller, D. Proprentner, M. Walker, C.T.J. Low, B. Shollock, H. Sun, P. Navabpour, Effect of chromium doping on high temperature tribological properties of silicon-doped diamond-like carbon films, Tribol. Int. 152 (2020), 106546, https://doi.org/10.1016/j.triboint.2020.106546.

[17] B.J. Rodriguez, P. Navabpour, D. Proprentner, M. Walker, H. Sun, T.L. Schiller, An alternative approach to the tribological analysis of Si-doped DLC coatings deposited with different bias voltages using Raman spectroscopy mapping, Emergent Mater. (2021), https://doi.org/10.1007/s42247-021-00263-w.

[18] S.C. Ray, W.F. Pong, P. Papakonstantinou, Iron, nitrogen and silicon doped diamond like carbon (DLC) thin films: a comparative study, Thin Solid Films 610 (2016) 42–47, https://doi.org/10.1016/j.tsf.2016.04.048.

[19] Y. Shibata, T. Kimura, S. Nakao, K. Azuma, Preparation of silicon-doped diamond-like carbon films with electrical conductivity by reactive high-power impulse magnetron sputtering combined with a plasma-based ion implantation system, Diam. Relat. Mater. 101 (2020), 107635, https://doi.org/10.1016/j.diamond.2019.107635.

[20] A. Erdemir, O.L. Eryilmaz, G. Fenske, Synthesis of diamondlike carbon films with superlow friction and wear properties, J. Vac. Sci. Technol. A Vacuum, Surfaces, Film 18 (2000) 1987, https://doi.org/10.1116/1.582459.

[21] Y. Liu, A. Erdemir, E.I. Meletis, A study of the wear mechanism of diamond-like carbon films 1, Surf. Coatings Technol. 82 (1996) 48–56, https://doi.org/10.1016/0257-8972(95)02623-1.

[22] N. Ohtake, M. Hiratsuka, K. Kanda, H. Akasaka, M. Tsujioka, K. Hirakuri, A. Hirata, T. Ohana, H. Inaba, M. Kano, H. Saitoh, Properties and classification of diamond-like carbon films, Materials (Basel) 14 (2021) 1–26, https://doi.org/10.3390/ma14020315.

[23] X. Chen, Y. Du, Y.W. Chung, Commentary on using H/E and H3/E2 as proxies for fracture toughness of hard coatings, Thin Solid Films. (2019), https://doi.org/10.1016/j.tsf.2019.04.040.

[24] A. Leyland, A. Matthews, On the significance of the H/E ratio in wear control: a nanocomposite coating approach to optimised tribological behaviour, Wear 246 (2000) 1–11, https://doi.org/10.1016/S0043-1648(00)00488-9.

[25] A. Leyland, A. Matthews, Design criteria for wear-resistant nanostructured and glassy-metal coatings, Surf. Coatings Technol. 177–178 (2004) 317–324, https://doi.org/10.1016/j.surfcoat.2003.09.011.

[26] Y.T. Cheng, Z. Li, C.M. Cheng, Scaling relationships for indentation measurements, Philos. Mag. A Phys. Condens. Matter, Struct. Defects Mech. Prop. 82 (2002) 1821–1829, https://doi.org/10.1080/01418610208235693.

[27] W. Ni, Y.T. Cheng, M.J. Lukitsch, A.M. Weiner, L.C. Lev, D.S. Grummon, Effects of the ratio of hardness to Young's modulus on the friction and wear behavior of bilayer coatings, Appl. Phys. Lett. 85 (2004) 4028–4030, https://doi.org/10.1063/1.1811377.

[28] K.L. Johnson, Contact Mechanics, Cambridge University Press, 1985.

[29] C. Donnet, A. Erdemir, Tribology of Diamond-Like Carbon Films, Springer US, Boston, MA, 2008, https://doi.org/10.1007/978-0-387-49891-1.

[30] F... Cui, D... Li, A review of investigations on biocompatibility of diamond-like carbon and carbon nitride films, Surf. Coatings Technol. 131 (2000) 481–487, https://doi.org/10.1016/S0257-8972(00)00809-4.

[31] M. Azzi, M. Paquette, J.A. Szpunar, J.E. Klemberg-Sapieha, L. Martinu, Tribocorrosion behaviour of DLC-coated 316L stainless steel, Wear. 267 (2009) 860–866. doi:10.1016/j.wear.2009.02.006.

[32] A. Grill, Diamond-like carbon: state of the art, Diam. Relat. Mater. 8 (1999) 428–434, https://doi.org/10.1016/S0925-9635(98)00262-3.

[33] B.D. Beake, T. Liskiewicz, Nanomechanical Characterization of Carbon Films, Appl. Nanoindentation Adv. Mater. (2017) 19–68, https://doi.org/10.1002/9781119084501.ch2.

[34] S.V. Johnston, S.V. Hainsworth, Effect of DLC coatings on wear in automotive applications, Surf. Eng. 21 (2005) 67–71, https://doi.org/10.1179/174329405x30039.

[35] B.D. Beake, M.I. Davies, T.W. Liskiewicz, V.M. Vishnyakov, S.R. Goodes, Nano-scratch, nanoindentation and fretting tests of 5-80 nm ta-C films on Si(100), Wear 301 (2013) 575–582, https://doi.org/10.1016/j.wear.2013.01.073.

[36] B.D. Beake, S.R. Goodes, B. Shi, Nanomechanical and nanotribological testing of ultra-thin carbon-based and MoST films for increased MEMS durability, J. Phys. D. Appl. Phys. (2009) 42, https://doi.org/10.1088/0022-3727/42/6/065301.

[37] Y. Pauleau, Residual stresses in DLC films and adhesion to various substrates, in: tribol. Diamond-Like Carbon Film, Fundam. Appl. (2008) 102–136, https://doi.org/10.1007/978-0-387-49891-1_4.

[38] W. Tillmann, N.F. Lopes Dias, D. Stangier, Tribo-mechanical properties of CrC/a-C thin films sequentially deposited by HiPIMS and mfMS, Surf. Coatings Technol. 335 (2018) 173–180, https://doi.org/10.1016/j.surfcoat.2017.12.035.

[39] S. Yang, X. Li, N.M. Renevier, D.G. Teer, Tribological properties and wear mechanism of sputtered C/Cr coating, Surf. Coatings Technol 142–144 (2001) 85–93, https://doi.org/10.1016/S0257-8972(01)01147-1.

[40] M. Diesselberg, H.R. Stock, P. Mayr, Friction and wear behaviour of PVD chromium nitride supported carbon coatings, Surf. Coatings Technol 188–189 (2004) 612–616, https://doi.org/10.1016/j.surfcoat.2004.07.023.

[41] L.F. Bonetti, G. Capote, L.V. Santos, E.J. Corat, V.J. Trava-Airoldi, Adhesion studies of diamond-like carbon films deposited on Ti6Al4V substrate with a silicon interlayer, Thin Solid Films 515 (2006) 375–379, https://doi.org/10.1016/j.tsf.2005.12.154.

[42] L. Lin, H. Peng, Z. Liu, Synthesis challenges for graphene industry, Nat. Mater. 18 (2019) 520–524, https://doi.org/10.1038/s41563-019-0341-4.

[43] P.C.T. Ha, D.R. McKenzie, M.M.M. Bilek, E.D. Doyle, D.G. McCulloch, P.K. Chu, Control of stress and delamination in single and multi-layer carbon thin films prepared by cathodic arc and RF plasma deposition and implantation, Surf. Coatings Technol. 200 (2006) 6405–6408, https://doi.org/10.1016/j.surfcoat.2005.11.011.

[44] Â.E. Crespi, L.M. Leidens, V. Antunes, B.L. Perotti, A.F. Michels, F. Alvarez, C.A. Figueroa, Substrate bias voltage tailoring the interfacial chemistry of a-SiCx:H: a surprising improvement in adhesion of a-C:h thin films deposited on ferrous alloys controlled by oxygen, ACS Appl. Mater. Interfaces. (2019), https://doi.org/10.1021/acsami.9b03597 acsami.9b03597.

[45] F. Cemin, L.T. Bim, C.M. Menezes, M.E.H. Maia da Costa, I.J.R. Baumvol, F. Alvarez, C.A. Figueroa, The influence of different silicon adhesion interlayers on the tribological behavior of DLC thin films deposited on steel by EC-PECVD, Surf. Coatings Technol. 283 (2015) 115–121, https://doi.org/10.1016/j.surfcoat.2015.10.031.

[46] F. Cemin, C.D. Boeira, C.A. Figueroa, On the understanding of the silicon-containing adhesion interlayer in DLC deposited on steel, Tribol. Int. 94 (2016) 464–469, https://doi.org/10.1016/j.triboint.2015.09.044.

[47] F. Cemin, L.T. Bim, L.M. Leidens, M. Morales, I.J.R. Baumvol, F. Alvarez, C.A. Figueroa, Identification of the Chemical Bonding Prompting Adhesion of a-C:h Thin Films on Ferrous Alloy Intermediated by a SiCx:h Buffer Layer, ACS Appl. Mater. Interfaces. 7 (2015) 15909–15917, https://doi.org/10.1021/acsami.5b03554.

[48] E.R. Petry, C.D. Boeira, F. Cemin, L.M. Leidens, L.T. Bim, D.G. Larrude, M.E.H. Maia da Costa, C.A. Figueroa, Physicochemical structure of SiCx:h to improve DLC adhesion on steel, Surf. Eng. 32 (2016) 779–785, https://doi.org/10.1080/02670844.2016.1159277.

[49] H. Ronkainen, K. Holmberg, Environmental and thermal effects on the tribological performance of DLC coatings, in: tribol. Diamond-Like Carbon Film, Fundam. Appl. (2008) 155–200, https://doi.org/10.1007/978-0-387-49891-1_6.

[50] A. Grill, Review of the tribology of diamond-like carbon, Wear 168 (1993) 143–153, https://doi.org/10.1016/0043-1648(93)90210-D.

[51] S.K. Field, M. Jarratt, D.G. Teer, Tribological properties of graphite-like and diamond-like carbon coatings, Tribol. Int. 37 (2004) 949–956, https://doi.org/10.1016/j.triboint.2004.07.012.

[52] Y. Liu, L. Chen, B. Zhang, Z. Cao, P. Shi, Y. Peng, N. Zhou, J. Zhang, L. Qian, Key role of transfer layer in load dependence of friction on hydrogenated diamond-like carbon films in humid air and vacuum, Materials (Basel) 12 (2019) 1–12, https://doi.org/10.3390/ma12091550.

[53] K. Wang, J. Zhang, T. Ma, Y. Liu, A. Song, X. Chen, Y. Hu, R.W. Carpick, J. Luo, Unraveling the Friction Evolution Mechanism of Diamond-Like Carbon Film during Nanoscale Running-In Process toward Superlubricity, Small. 17 (2020), https://doi.org/10.1002/smll.202005607.

[54] X. Chen, J. Li, Superlubricity of carbon nanostructures, Carbon N. Y. 158 (2020) 1–23, https://doi.org/10.1016/j.carbon.2019.11.077.

[55] D. Berman, S.A. Deshmukh, S.K.R.S. Sankaranarayanan, A. Erdemir, A.V. Sumant, Macroscale superlubricity enabled by graphene nanoscroll formation, Science 348 (80) (2015) 1118–1122, https://doi.org/10.1126/science.1262024.

[56] W.G. Sawyer, K.J. Wahl, Accessing inaccessible interfaces: in situ approaches to materials tribology, MRS Bull 33 (2008) 1145–1150, https://doi.org/10.1557/mrs2008.244.

[57] K. Meine, T. Schneider, D. Spaltmann, E. Santner, The influence of roughness on friction Part I: the influence of a single step, Wear 253 (2002) 725–732, https://doi.org/10.1016/S0043-1648(02)00159-X.

[58] K. Meine, T. Schneider, D. Spaltmann, E. Santner, The influence of roughness on friction Part II. The influence of multiple steps, Wear 253 (2002) 733–738, https://doi.org/10.1016/S0043-1648(02)00160-6.

[59] E. Santner, D. Klaffke, K. Meine, C. Polaczyk, D. Spaltmann, Demonstration of topography modification by friction processes and vice versa, Tribol. Int. 39 (2006) 450–455, https://doi.org/10.1016/j.triboint.2005.04.029.

[60] E. Santner, D. Klaffke, K. Meine, C. Polaczyk, D. Spaltmann, Effects of friction on topography and vice versa, Wear 261 (2006) 101–106, https://doi.org/10.1016/j.wear.2005.09.028.

[61] M. Weidner, O. Borrero-López, M. Hoffman, A. Bendavid, P.J. Martin, Effect of substrate roughness on the contact damage of thin brittle films on brittle

[62] F.M. Borodich, E. Brousseau, A. Clarke, A. Pepelyshev, J.C. Sánchez-López, Roughness of Deposited Carbon-Based Coatings and Its Statistical Characteristics at Nano and Microscales, Front. Mech. Eng. 5 (2019) 1–13, https://doi.org/10.3389/fmech.2019.00024.

[63] A. Ali, K.K. Hirakuri, G. Friedbacher, Roughness and deposition mechanism of DLC films prepared by r.f. plasma glow discharge, Vacuum 51 (1998) 363–368, https://doi.org/10.1016/S0042-207X(98)00115-8.

[64] J. Jiang, R.D. Arnell, The effect of substrate surface roughness on the wear of DLC coatings, Wear 239 (2000) 1–9, https://doi.org/10.1016/S0043-1648(99)00351-8.

[65] P. Lindholm, S. Björklund, F. Svahn, Method and surface roughness aspects for the design of DLC coatings, Wear 261 (2006) 107–111, https://doi.org/10.1016/j.wear.2005.09.029.

[66] X.L. Peng, Z.H. Barber, T.W. Clyne, Surface roughness of diamond-like carbon films prepared using various techniques, Surf. Coatings Technol. 138 (2001) 23–32, https://doi.org/10.1016/S0257-8972(00)01139-7.

[67] G.M. Wilson, J.F. Smith, J.L. Sullivan, A nanotribological study of thin amorphous C and Cr doped amorphous C coatings, Wear 265 (2008) 1633–1641, https://doi.org/10.1016/j.wear.2008.03.017.

[68] L. Chen, M. Yang, J. Yu, L. Qian, Z. Zhou, Nanofretting behaviours of ultrathin DLC coating on Si(100) substrate, Wear 271 (2011) 1980–1986, https://doi.org/10.1016/j.wear.2010.11.016.

[69] J.X. Yu, L.M. Qian, B.J. Yu, Z.R. Zhou, Nanofretting behaviors of monocrystalline silicon (1 0 0) against diamond tips in atmosphere and vacuum, Wear 267 (2009) 322–329, https://doi.org/10.1016/j.wear.2008.11.008.

[70] B.D. Beake, T.W. Liskiewicz, J.F. Smith, Deformation of Si(100) in spherical contacts - Comparison of nano-fretting and nano-scratch tests with nano-indentation, Surf. Coatings Technol. 206 (2011) 1921–1926, https://doi.org/10.1016/j.surfcoat.2011.10.035.

[71] S. Achanta, D. Drees, J.P. Celis, Friction and nanowear of hard coatings in reciprocating sliding at milli-Newton loads, in: wear, Elsevier (2005) 719–729, https://doi.org/10.1016/j.wear.2005.02.078.

[72] D. Drees, J.P. Celis, S. Achanta, Friction of thin coatings on three length scales under reciprocating sliding, Surf. Coatings Technol 188–189 (2004) 511–518, https://doi.org/10.1016/j.surfcoat.2004.07.008.

[73] S. Achanta, D. Drees, J.P. Celis, Friction from nano to macroforce scales analyzed by single and multiple-asperity contact approaches, Surf. Coatings Technol. 202 (2008) 6127–6135, https://doi.org/10.1016/j.surfcoat.2008.07.020.

[74] B. Bhushan, H. Liu, S.M. Hsu, Adhesion and friction studies of silicon and hydrophobic and low friction films and investigation of scale effects, J. Tribol. 126 (2004) 583–590, https://doi.org/10.1115/1.1739407.

[75] M. Pandey, D. Bhatacharyya, D.S. Patil, K. Ramachandran, N. Venkatramani, Diamond-like carbon coatings: AFM and ellipsometric studies, Surf. Coatings Technol. 182 (2004) 24–34, https://doi.org/10.1016/S0257-8972(03)00876-4.

[76] Z. Nibennanoune, D. George, F. Antoni, S. Ahzi, D. Ruch, J. Gracio, Y. Remond, Improving diamond coating on Ti6Al4V substrate using a diamond like carbon interlayer: raman residual stress evaluation and AFM analyses, Diam. Relat. Mater. 22 (2012) 105–112, https://doi.org/10.1016/j.diamond.2011.12.023.

[77] L.Y. Ostrovskaya, Studies of diamond and diamond-like film surfaces using XAES, AFM and wetting, Vacuum 68 (2002) 219–238, https://doi.org/10.1016/S0042-207X(02)00460-8.

[78] H.S. Zhang, J.L. Endrino, A. Anders, Comparative surface and nano-tribological characteristics of nanocomposite diamond-like carbon thin films doped by silver, Appl. Surf. Sci. 255 (2008) 2551–2556, https://doi.org/10.1016/j.apsusc.2008.07.193.

[79] D. Drees, J.P. Celis, S. Achanta, Friction of thin coatings on three length scales under reciprocating sliding, Surf. Coatings Technol. 188–189 (2004) 511–518. doi:10.1016/j.surfcoat.2004.07.008.

[80] D.L. Burris, W.G. Sawyer, Addressing practical challenges of low friction coefficient measurements, Tribol. Lett. 35 (2009) 17–23, https://doi.org/10.1007/s11249-009-9438-2.

[81] M. Moseler, P. Cumbsch, C. Casiraghi, A.C. Ferrari, J. Robertson, Materials science: the ultrasmoothness of diamond-like carbon surfaces, Science 309 (80) (2005) 1545–1548, https://doi.org/10.1126/science.1114577.

[82] E. Neyts, A. Bogaerts, R. Gijbels, J. Benedikt, M.C.M. Van De Sanden, Molecular dynamics simulations for the growth of diamond-like carbon films from low kinetic energy species, Diam. Relat. Mater. 13 (2004) 1873–1881, https://doi.org/10.1016/j.diamond.2004.05.011.

[83] T.B. Ma, Y.Z. Hu, H. Wang, X. Li, Microstructural and stress properties of ultrathin diamondlike carbon films during growth: molecular dynamics simulations, Phys. Rev. B - Condens. Matter Mater. Phys. 75 (2007) 1–8, https://doi.org/10.1103/PhysRevB.75.035425.

[84] X. Li, P. Ke, K.R. Lee, A. Wang, Molecular dynamics simulation for the influence of incident angles of energetic carbon atoms on the structure and properties of diamond-like carbon films, Thin Solid Films 552 (2014) 136–140, https://doi.org/10.1016/j.tsf.2013.12.012.

[85] K. Hayashi, K. Tezuka, N. Ozawa, T. Shimazaki, K. Adachi, M. Kubo, Tribochemical reaction dynamics simulation of hydrogen on a diamond-like carbon surface based on tight-binding quantum chemical molecular dynamics, J. Phys. Chem. C. 115 (2011) 22981–22986, https://doi.org/10.1021/jp207065n.

[86] X. Li, P. Ke, A. Wang, Probing the stress reduction mechanism of diamond-like carbon films by incorporating Ti, Cr, or W carbide-forming metals: ab initio

molecular dynamics simulation, J. Phys. Chem. C. 119 (2015) 6086–6093, https://doi.org/10.1021/acs.jpcc.5b00058.

[87] F.P. Bowden, D. Tabor, The Friction and Lubrication of Solids, Oxford Clarendon Press, 1950.

[88] J.K. Xiao, L. Zhang, K.C. Zhou, X.P. Wang, Microscratch behavior of copper-graphite composites, Tribol. Int. 57 (2013) 38–45, https://doi.org/10.1016/j.triboint.2012.07.004.

[89] B.D. Beake, A.J. Harris, T.W. Liskiewicz, Review of recent progress in nanoscratch testing, Tribol. - Mater. Surfaces Interfaces. 7 (2013) 87–96, https://doi.org/10.1179/1751584x13Y.0000000037.

[90] B.D. Beake, S.P. Lau, Nanotribological and nanomechanical properties of 5–80nm tetrahedral amorphous carbon films on silicon, Diam. Relat. Mater. 14 (2005) 1535–1542, https://doi.org/10.1016/j.diamond.2005.04.002.

[91] NANOINDENT-plus, NANOINDENT-PLUS project Standardising the nano-scratch test, NMP-2012-CSA-6-319208., (2012).

[92] M. Bai, L. Yang, J. Li, L. Luo, S. Sun, B. Inkson, Mechanical and tribological properties of Si and W doped diamond like carbon (DLC) under dry reciprocating sliding conditions, Wear 484–485 (2021), 204046, https://doi.org/10.1016/j.wear.2021.204046.

[93] S.J. McMaster, T.W. Liskiewicz, B.D. Beake, A. Neville, Probing Fatigue Resistance in Multi-layer DLC Coatings by Micro-impact: correlation to Erosion Tests, Surf. Coatings Technol. 402 (2020), 126319, https://doi.org/10.1016/j.surfcoat.2020.126319.

[94] Oerlikon Balzers, Coated components: great Performance and reliability, 2010.

[95] ISO, ISO 14577-1:2015 Metallic materials – Instrumented indentation test for hardness and materials parameters – Part 1: test method, (2015) 58.

[96] ISO, ISO 14577-4:2016 Metallic materials — Instrumented indentation test of hardness and materials parameters Part 1 : test method, (2016) 19.

[97] CEN/TS, 17629:2021 Nanotechnologies — Nano- and micro- scale scratch testing, (2021).

[98] B.D. Beake, V.M. Vishnyakov, T.W. Liskiewicz, Integrated Nanomechanical Characterisation of Hard Coatings. Prot. Thin Coatings Technol, CRC Press, 2021, pp. 95–139, https://doi.org/10.1201/9781003088349-4.

[99] T.W. Liskiewicz, B.D. Beake, J.F. Smith, In situ accelerated micro-wear - A new technique to fill the measurement gap, Surf. Coatings Technol. 205 (2010) 1455–1459, https://doi.org/10.1016/j.surfcoat.2010.07.109.

[100] T. Liskiewicz, S. Fouvry, Development of a friction energy capacity approach to predict the surface coating endurance under complex oscillating sliding conditions, Tribol. Int. 38 (2005) 69–79, https://doi.org/10.1016/j.triboint.2004.06.002.

[101] R. Rybiak, S. Fouvry, T. Liskiewicz, B. Wendler, Fretting wear of a TiN PVD coating under variable relative humidity conditions—Development of a 'composite' wear law, Surf. Coatings Technol. 202 (2008) 1753–1763, https://doi.org/10.1016/J.SURFCOAT.2007.07.103.

[102] J. Laporte, O. Perrinet, S. Fouvry, Prediction of the electrical contact resistance endurance of silver-plated coatings subject to fretting wear, using a friction energy density approach, Wear 330–331 (2015) 170–181, https://doi.org/10.1016/J.WEAR.2014.12.006.

[103] A. Singh, M. Dao, L. Lu, S. Suresh, Deformation, structural changes and damage evolution in nanotwinned copper under repeated frictional contact sliding, ACTA Mater 59 (2011) 7311–7324, https://doi.org/10.1016/j.actamat.2011.08.014.

[104] B.D. Beake, S.R. Goodes, J.F. Smith, R. Madani, C.A. Rego, R.I. Cherry, T. Wagner, Investigating the fracture resistance and adhesion of DLC films with micro-impact testing, Diam. Relat. Mater. 11 (2002) 1606–1609, https://doi.org/10.1016/S0925-9635(02)00107-3.

[105] B.D. Beake, A.A. Ogwu, T. Wagner, Influence of experimental factors and film thickness on the measured critical load in the nanoscratch test, Mater. Sci. Eng. A. 423 (2006) 70–73, https://doi.org/10.1016/J.MSEA.2005.09.121.

[106] O. Zwörner, H. Hölscher, U.D. Schwarz, R. Wiesendanger, The velocity dependence of frictional forces in point-contact friction, Appl. Phys. A Mater. Sci. Process. 66 (1998) 263–267, https://doi.org/10.1007/s003390051142.

[107] T.Y. Tsui, G.M. Pharr, W.C. Oliver, C.S. Bhatia, R.L. White, S. Anders, A. Anders, I.G. Brown, Nanoindentation and nanoscratching of hard carbon coatings for magnetic disks, Mater. Res. Soc. Symp. - Proc., Mater. Res. Soc. (1995) 447–452, https://doi.org/10.1557/proc-383-447.

[108] Y.W. Rhee, H.W. Kim, Y. Deng, B.R. Lawn, Brittle Fracture versus Quasi Plasticity in Ceramics: a Simple Predictive Index, J. Am. Ceram. Soc. 84 (2001) 561–565, https://doi.org/10.1111/J.1151-2916.2001.TB00698.X.

[109] B.D. Beake, V.M. Vishnyakov, A.J. Harris, Relationship between mechanical properties of thin nitride-based films and their behaviour in nano-scratch tests, Tribol. Int. 44 (2011) 468–475, https://doi.org/10.1016/j.triboint.2010.12.002.

[110] B.D. Beake, V.M. Vishnyakov, A.J. Harris, Nano-scratch testing of (Ti,Fe)Nx thin films on silicon, Surf. Coatings Technol. 309 (2017) 671–679, https://doi.org/10.1016/J.SURFCOAT.2016.11.024.

[111] H. Kitsunai, K. Kato, K. Hokkirigawa, H. Inoue, The transitions between microscopic wear modes during repeated sliding friction observed by a scanning electron microscope tribosystem, Wear 135 (1990) 237–249, https://doi.org/10.1016/0043-1648(90)90028-9.

[112] K. Hokkirigawa, K. Kato, Z.Z. Li, The effect of hardness on the transition of the abrasive wear mechanism of steels, WEAR 123 (1988) 241–251, https://doi.org/10.1016/0043-1648(88)90102-0.

[113] D.F. Diao, K. Kato, K. Hayashi, The maximum tensile stres on a hard coating under sliding friction, Tribol. Int. 27 (1994) 267–272, https://doi.org/10.1016/0301-679X(94)90006-X.

[114] K. Kato, Microwear mechanisms of coatings, Surf. Coatings Technol. 76–77 (1995) 469–474, https://doi.org/10.1016/0257-8972(95)02570-7.

[115] F. Zhang, B. Meng, Y. Geng, Y. Zhang, Z. Li, Friction behavior in nanoscratching of reaction bonded silicon carbide ceramic with Berkovich and sphere indenters, Tribol. Int. 97 (2016) 21–30, https://doi.org/10.1016/j.triboint.2016.01.013.

[116] J.D. Kamminga, G.C.A.M. Janssen, Experimental discrimination of plowing friction and shear friction, Tribol. Lett. 25 (2007) 149–152, https://doi.org/10.1007/s11249-006-9135-3.

[117] J. Goddard, H. Wilman, A theory of friction and wear during the abrasion of metals, Wear 5 (1961) 114–135.

[118] S. Lafaye, M. Troyon, On the friction behaviour in nanoscratch testing, Wear 261 (2006) 905–913, https://doi.org/10.1016/j.wear.2006.01.036.

[119] G. Pagnoux, S. Fouvry, M. Peigney, B. Delattre, G. Mermaz-Rollet, Mechanical Behavior of DLC coatings under various scratch conditions, Proc. 3rd Int. Conf. Fract. Fatigue Wear 2 (2014) 308–313.

[120] G.M. Wilson, J.F. Smith, J.L. Sullivan, A DOE nano-tribological study of thin amorphous carbon-based films, Tribol. Int. 42 (2009) 220–228, https://doi.org/10.1016/j.triboint.2008.06.006.

[121] G.M. Wilson, J.L. Sullivan, An investigation into the effect of film thickness on nanowear with amorphous carbon-based coatings, Wear 266 (2009) 1039–1043, https://doi.org/10.1016/j.wear.2008.12.001.

[122] G.M. Wilson, An Investigation of Thin Amorphous Carbon-Based Sputtered Coatings For MEMS and Micro-Engineering Applications, Aston University, 2008, https://doi.org/10.48780/PUBLICATIONS.ASTON.AC.UK.00008105.

[123] B.D. Beake, T.W. Liskiewicz, Comparison of nano-fretting and nano-scratch tests on biomedical materials, Tribol. Int. (2013) 123–131, https://doi.org/10.1016/j.triboint.2012.08.007.

[124] S. Korres, T. Feser, M. Dienwiebel, A new approach to link the friction coefficient with topography measurements during plowing, Wear 303 (2013) 202–210, https://doi.org/10.1016/j.wear.2013.03.010.

[125] B.D. Beake, S.J. McMaster, T.W. Liskiewicz, A. Neville, Influence of Si- and W-doping on micro-scale reciprocating wear and impact performance of DLC coatings on hardened steel, Tribol. Int. (2021), 107063, https://doi.org/10.1016/j.triboint.2021.107063.

[126] G.M. Hamilton, L.E. Goodman, The Stress Field Created by a Circular Sliding Contact, J. Appl. Mech. 33 (1966) 371–376, https://doi.org/10.1115/1.3625051.

[127] T. Chudoba, N. Schwarzer, F. Richter, Steps towards a mechanical modeling of layered systems, Surf. Coatings Technol. 154 (2002) 140–151, https://doi.org/10.1016/S0257-8972(02)00016-6.

[128] K. Holmberg, H. Ronkainen, A. Laukkanen, K. Wallin, Friction and wear of coated surfaces — Scales, modelling and simulation of tribomechanisms, Surf. Coatings Technol. 202 (2007) 1034–1049, https://doi.org/10.1016/J.SURFCOAT.2007.07.105.

[129] K. Holmberg, H. Ronkainen, A. Laukkanen, K. Wallin, A. Erdemir, O. Eryilmaz, Tribological analysis of TiN and DLC coated contacts by 3D FEM modelling and stress simulation, Wear 264 (2008) 877–884, https://doi.org/10.1016/J.WEAR.2006.12.084.

[130] N. Schwarzer, Q.H. Duong, N. Bierwisch, G. Favaro, M. Fuchs, P. Kempe, B. Widrig, J. Ramm, Optimization of the Scratch Test for specific coating designs, Surf. Coatings Technol. 206 (2011) 1327–1335, https://doi.org/10.1016/j.surfcoat.2011.08.051.

[131] K.I. Schiffmann, A. Hieke, Analysis of microwear experiments on thin DLC coatings: friction, wear and plastic deformation, Wear 254 (2003) 565–572, https://doi.org/10.1016/S0043-1648(03)00188-1.

[132] K.I. Schiffmann, Phenomena in microwear experiments on metal-free and metal-containing diamond-like carbon coatings: friction, wear, fatigue and plastic deformation, Surf. Coatings Technol. 177–178 (2004) 453–458, https://doi.org/10.1016/j.surfcoat.2003.08.064.

[133] P. Stoyanov, R.R. Chromik, S. Gupta, J.R. Lince, Micro-scale sliding contacts on Au and Au-MoS2 coatings, Surf. Coatings Technol. 205 (2010) 1449–1454, https://doi.org/10.1016/j.surfcoat.2010.07.026.

[134] M.G. Gee, J.W. Nunn, A. Muniz-Piniella, L.P. Orkney, Micro-tribology experiments on engineering coatings, Wear 271 (2011) 2673–2680, https://doi.org/10.1016/j.wear.2011.02.031.

[135] F.C. Hsia, F.M. Elam, D. Bonn, B. Weber, S.E. Franklin, Wear particle dynamics drive the difference between repeated and non-repeated reciprocated sliding, Tribol. Int. 142 (2020), 105983, https://doi.org/10.1016/j.triboint.2019.105983.

[136] K. Holmberg, A. Laukkanen, H. Ronkainen, R. Waudby, G. Stachowiak, M. Wolski, P. Podsiadlo, M. Gee, J. Nunn, C. Gachot, L. Li, Topographical orientation effects on friction and wear in sliding DLC and steel contacts, part 1: experimental, Wear 330–331 (2015) 3–22, https://doi.org/10.1016/j.wear.2015.02.014.

[137] T.W. Liskiewicz, B.D. Beake, N. Schwarzer, M.I. Davies, Short note on improved integration of mechanical testing in predictive wear models, Surf. Coatings Technol. 237 (2013) 212–218, https://doi.org/10.1016/j.surfcoat.2013.07.044.